

DESIGN OF A WIDEBAND PROBE FOR THE MEASUREMENT OF
THE ELECTRICAL PARAMETERS OF MATERIALS

A Thesis
presented to
the Faculty of Engineering
at Notre Dame University-Louaize

In Partial Fulfillment
of the Requirements for the Degree
Master of Science
in Electrical and Computer Engineering (MSECE)

by
CHRISTELLE NASRANY
MARCH 2019

Notre Dame University - Louaize
Faculty of Engineering
Department of Electrical, Computer and Communication Engineering

We hereby approve the thesis of

Christelle Nasrany

Candidate for the degree of Master of Science in Electrical and Computer Engineering




Dr. Elias Nassar Supervisor, Chair



Dr. Semaan Georges Committee Member



Dr. Nassar Mendalek Committee Member



Dr. Youssef Tawfik Committee Member

ACKNOWLEDGMENTS

My primary thanks are to GOD for giving me the peace, persistence and blessings from the beginning of my work in the last three years, till this moment. God was leading me while I was working on this thesis, and was helping me to take the right decisions and follow the right plan.

Warm appreciations to the one I owe lots of credit to, to the Doctor who was charged to pursue my evolution through this thesis in spite of his busy schedule. I would like to express my appreciation to Dr. Elias Nassar, my advisor in this thesis, who was always ready to help me. Dr. Nassar solved many of my problems and deserves much more than my thanks.

Furthermore, I am very grateful to all professors of Electrical, Computer and Communications Engineering Department who played a major role in my academic life and graduate studies, and made me reach the level at which I am now. Thanks to each and every member of the faculty of engineering, Dean, Chairman, Doctors and staff, they all leaved a trace in my five academic years of engineering and three years of graduate studies, and I grasped different types of knowledge through them.

Finally, my thanks are extended to reach my parents and family. It is impossible for me to ignore the importance of the presence of my parents mainly, who were encouraging me to persist and achieve my goals, and were supporting me through all the difficulties I faced. My hard work and persistence are because of their inspiration and motivation. This book will be dedicated to my parents who made me reach this stage.

Last but not least, this project has been funded with support from the National Council for Scientific Research (CNRS) in Lebanon, and it is elaborated by three different universities: Notre Dame University-Louaize NDU, Lebanese University LU and the American University of Beirut AUB.

ABSTRACT

The purpose of this thesis is to design and test a device that measures the electrical parameters of a certain material.

This device can have different applications, like assisting in landmines detection, agricultural or construction purposes. In order to measure the electrical parameters, this device or probe uses two wideband planar dipole antennas that operate in the frequency range between 3 and 6 GHz. The transmitted signal between the antennas, (S_{21}), is measured and then compared to a database obtained by simulating different materials using the Finite Difference Time Domain Method.

Based on this comparison, one can extract the dielectric constant and conductivity of the material. Preliminary results show that this probe can be used with reasonable accuracy to measure in-situ the electrical parameters of soil.

TABLE OF CONTENTS

ACKNOWLEDGMENTS	iii
ABSTRACT.....	v
TABLE OF CONTENTS.....	vi
LIST OF TABLES	viii
LIST OF FIGURES	ix
Chapter 1 - INTRODUCTION	1
1.1 Background	1
1.2 Main Purpose.....	2
1.3 Measurement of Material Electrical Parameters	2
1.4 Outline.....	7
Chapter 2 – ANTENNAS AND FDTD METHOD	9
2.1 Antennas Theory	9
2.2 Antenna Selection	10
2.3 Theory of FDTD.....	15
2.4 Deriving Equations.....	17
Chapter 3 - PROBE DESIGN	20
3.1 Design Block Diagram	20
3.2 Triangular Monopole Antennas	22
3.2.1 Building the Geometry	22
3.2.2 Defining the Signal.....	26
3.2.3 Requesting the Results.....	26
3.2.4 Extraction and Processing of the Results using MATLAB.....	31
3.3 Circular Monopole Antenna.....	33
3.4 Planar Dipole Antenna	40
3.4.1 Theoretical	40
3.4.2 XFDTD Simulation	43
Chapter 4 - MEASUREMENTS	49
4.1 Electrical Parameters Extracted	49
4.2 Extraction of Parameters	68
Chapter 5 - SUMMARY, CONCLUSION AND FUTURE WORK.....	75
5.1 Summary	75
5.2 Conclusion.....	75
5.3 Future Work	76
APPENDIX A	78
APPENDIX B	84

REFERENCES 89

LIST OF TABLES

Table 3.1 - Comparison of S_{21}	32
Table 3.2 - Comparison of S_{21} at 4 GHz.....	39
Table 3.3 - Comparison of S_{21} at 5 GHz.....	40
Table 4.1 - S_{21} Magnitude and Phase Normalized Database at 3 GHz.....	69
Table 4.2 - S_{21} Magnitude and Phase Normalized Database at 4 GHz.....	69
Table 4.3 - S_{21} Magnitude and Phase Normalized Database at 5 GHz.....	69
Table 4.4 - S_{21} Magnitude and Phase Normalized Database at 6 GHz.....	69
Table 4.5 – Ottawa Sand Measurements.....	70
Table 4.6 – Sandstone Measurements.....	71
Table 4.7 – Clay Measurements.....	73
Table 4.8 – Soil Sample Measurements.....	73

LIST OF FIGURES

Figure 1.1 -Network Analyzer [5]	3
Figure 1.2 - LCRs	4
Figure 2.1 - Horn Antenna Radiation Pattern	10
Figure 2.2 - Dipole Antenna Radiation Pattern	10
Figure 2.3 - Resonance of Circular UWB Antennas.....	14
Figure 2.4 - Antennas Geometries	15
Figure 2.5 - VSWR vs. Frequency.....	15
Figure 2.6 – 1D FDTD Implemetation	18
Figure 2.7 – 3D indices of Electric Field.....	19
Figure 2.8 - Yee Cell in 3D System.....	19
Figure 3.1 - Design Sketch.....	21
Figure 3.2 – Detailed Design	22
Figure 3.3 - Plot of DGP vs. Time	23
Figure 3.4 - Plot of DGP vs. frequency	23
Figure 3.5 - Rectangular Medium.....	24
Figure 3.6 - Complete Geometry	25
Figure 3.7 - Triangular Monopole Antenna.....	25
Figure 3.8 - Source Definition	26
Figure 3.9 – Transmitted Field vs. Time.....	27
Figure 3.10 - Received Signal in Free Space.....	27
Figure 3.11 - S_{21} in Free Space	28
Figure 3.12 - Received Signal in Soil Type 1	29

Figure 3.13 - S_{21} in Soil Type 1	29
Figure 3.14 - Received Signal in Soil Type 2	30
Figure 3.15 - S_{21} in Soil Type 2	30
Figure 3.16 - S_{11} vs. Frequency	31
Figure 3.17 - S_{21} Magnitude vs. Frequency	32
Figure 3.18 - S_{21} Phase vs. Frequency	32
Figure 3.19 - Circular Monopole Antenna - Front View	33
Figure 3.20 - Circular Monopole Antenna - Back View	34
Figure 3.21 - Design Geometry	34
Figure 3.22 - Transmitted Signal vs. Time in Free Space	35
Figure 3.23 - Received Signal vs. Time in Free Space	35
Figure 3.24 - S_{21} Magnitude vs. Frequency in Free Space	36
Figure 3.25 - S_{11} vs. Frequency in Free Space.....	36
Figure 3.26 - First Snapshot of the Field Propagation in Free Space	37
Figure 3.27 - Second Snapshot of the Field Propagation in Free Space.....	37
Figure 3.28 - Third Snapshot of the Field Propagation in Free Space.....	38
Figure 3.29 - 2D Pattern - Constant Phi 90 Plane.....	38
Figure 3.30 - 2D Pattern - Constant Phi 0 Plane.....	39
Figure 3.31 - 3D Pattern.....	39
Figure 3.32 - Planar Elliptical Dipole Antenna	41
Figure 3.33 - Deepace Antenna	42
Figure 3.34 - Deepace Antenna Ground Plane	43
Figure 3.35 - Deepace Antenna S_{11}	43
Figure 3.36 - AutoCAD Drawing of Deepace Antenna.....	44
Figure 3.37 - Deepace System	44

Figure 3.38 - S_{11} of Deepace Antenna	45
Figure 3.39 - S_{21} Deepace Free Space	46
Figure 3.40 - S_{21} in Soil Type1	46
Figure 3.41 - S_{21} in Soil Type2	46
Figure 3.42 - S_{21} in Soil Type3	47
Figure 3.43 - Deepace E Plane.....	47
Figure 3.44 - Deepace H Plane	48
Figure 3.45 - Deepace 3D Pattern.....	48
Figure 4.1 - S_{11} Vector Measured	50
Figure 4.2 - S_{21} Measuring Position.....	50
Figure 4.3 - S_{21} Vector Measured	51
Figure 4.4 - S_{21} Positioning Rotated	52
Figure 4.5 - S_{21} Second Positioning Rotated	52
Figure 4.6 - E Plane Measurement Position.....	53
Figure 4.7 – Normalized E Plane Measured at 4 GHz.....	54
Figure 4.8 – Normalized E Plane Measured at 5 GHz.....	54
Figure 4.9 - H Plane Measurement Position	55
Figure 4.10 - Anechoic Chamber Antenna Position	55
Figure 4.11 – Normalized H Plane Measured at 4 GHz	56
Figure 4.12 – Normalized H Plane Measured at 5 GHz	56
Figure 4.13 – Normalized H Plane Measured at 2 GHz	57
Figure 4.14 - Calibration of Network Analyzer.....	58
Figure 4.15 - S_{11} Measured by Network Analyzer	58
Figure 4.16 - S_{21} Measured by Network Analyzer	59
Figure 4.17 - Free Space Position	60

Figure 4.18 - Free Space Phase of S_{21}	60
Figure 4.19 - Absorber Positioning.....	61
Figure 4.20 - Phase of S_{21} in Absorber	61
Figure 4.21 - System Setting Out.....	62
Figure 4.22 - S_{21} of Ottawa Sand	63
Figure 4.23 - Complete Probe with Antennas.....	64
Figure 4.24 - $ S_{21} $ vs. frequency in Ottawa Sand at Different Depths	65
Figure 4.25 - S_{21} Phase vs. Frequency in Ottawa Sand at Different Depths.....	65
Figure 4.26 - Beeswax Measurement.....	66
Figure 4.27 - Sand Stone.....	67
Figure 4.28 – Sand Stone Measurements.....	67
Figure 4.29 – Clay Sample.....	68
Figure 4.30 - S_{21} vs. Frequency in Free Space and Sandstone	71
Figure 4.31 - Normalized Magnitude of S_{21} in Sand Stone	71
Figure 4.32 - Normalized Phase of S_{21} in Sandstone.....	72
Figure 4.33 – Magnitude of S_{21} vs. Frequency in Clay	72
Figure 4.34 - Magnitude of S_{21} vs. Frequency in Random Soil.....	74

Chapter 1 - INTRODUCTION

In this Chapter, the main purpose of this report is presented in addition to the motivations that led to its preparation. Furthermore, an outline of the main Chapters included in this report is given.

1.1 Background

As of 2011 there were approximately 400,000 landmines in Lebanon according to the Lebanese Army, and as per a 2003 national landmine impact survey conducted by the British charity mines advisory group. Most of those mines are implanted in the south area of Lebanon, yet their exact locations are still not known. The total endangered lands have an area of 95km² of which 46% are still contaminated with landmines. The total area of land contaminated with cluster bombs was 55km² of which 18.2% are still contaminated and the remaining were completely cleared. Those mines were originated from various wars between 1975 and 1990, meaning that they are aged between 15 and 50 years, according to military forces.

Many types of landmines exist in Lebanon, as AP or Anti Personal landmines designed in the purpose of injuring persons, and AT or Anti-Tank mines mostly used for damaging vehicles. As the time is passing, it is getting harder to detect the locations of the landmines because they are being affected by many environmental issues, leading to some material degradation and causing the outer casing components to break down. Those environmental influences include fire damage, weathering of plastics and corrosion of metals. Consequently, hidden landmines are creating serious problems for

all Lebanese civilians that are endangered to face landmines' risks, especially as they move to unpopulated areas.

Various organizations and governments are helping Lebanon to find a way to overcome the problem of mine clearance, with best accuracy and less false alarm rate. The methods currently used rely on manual detection by trained personnel. Their progress is too slow and they present a high level of danger to the operator. In addition, land mines are causing injuries to farmers and to the general public. It is noticeable that 11.9% of the handicapped persons were recorded for being victims of wars including landmines accidents [1,2,3].

1.2 Main Purpose

Ground Penetrating Radar (GPR) can be an effective tool to speed up the detection of landmines. However, there is a need to determine the soil parameters of the area where the landmines are buried. The project's goal is to find a new way or a new device that can determine the soil parameters, in order to be able to find the landmines with lower false alarm rates.

1.3 Measurement of Material Electrical Parameters

A material that can store energy when subjected to an external field is called a dielectric. The dielectric constant of a material is a complex value that has a real part for the storing capacity of the energy from the external field, and an imaginary part responsible for the loss and dissipative figure of the material. This dielectric constant, usually called k , is equivalent to relative permittivity ϵ_r .

The permeability of a material, represented by μ , describes the interaction of a material with a magnetic field. It is also described as the ability of a material to support the presence of a magnetic field within itself, indicating the degree of magnetization that a material obtains in response to an applied magnetic field [4,5,6].

Most of the measurement methods aiming to find the permittivity and permeability of a material, or even for other electrical parameters, rely mainly on the following components. To start with network analyzers, a vector network analyzer consists of a signal source, a receiver and a display. The source launches a signal at a single frequency to the material under test. The receiver is tuned to that frequency to detect the reflected and transmitted signals from the material. The measured response produces the magnitude and phase data at that frequency. The source is then stepped to the next frequency and the measurement is repeated to display the reflection and transmission measurement response as a function of frequency [5].

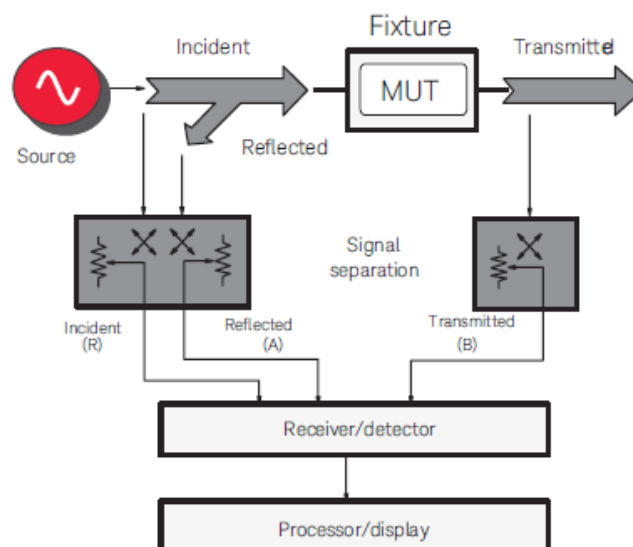


Figure 1.1 -Network Analyzer [5]

Impedance analyzers and LCR meters are used to measure the material properties at lower frequencies. The material is stimulated with an AC source and the actual voltage across the material is monitored. Material test parameters are derived by knowing the dimensions of the material and by measuring its capacitance and dissipation factor. Figure 1.2 shows the different devices used in different frequency ranges [5].

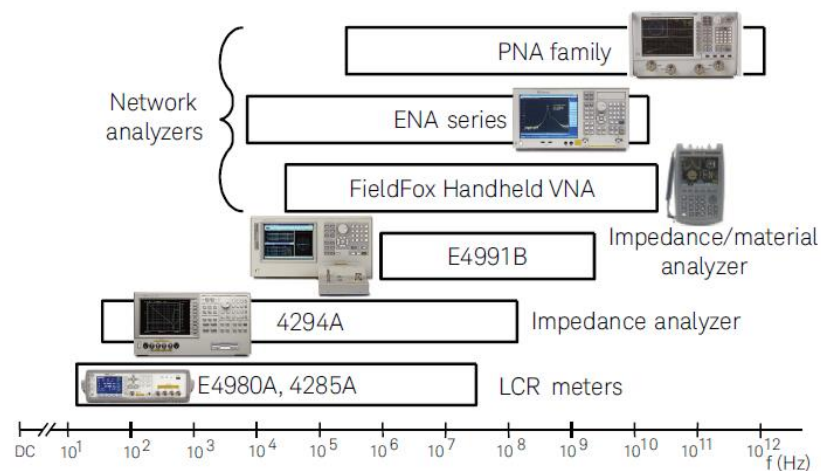


Figure 1.2 - LCRs

Some measurement techniques are described in [7], from which we can extract brief descriptions as follows:

- The open-ended coaxial probe is a cut off section of transmission line. The material is measured by immersing the probe into a liquid or touching it to the flat face of a solid material. The fields at the probe end change and the reflected signal (S_{11}) can be measured and related to ϵ_r .
- Transmission line methods involve placing the material inside a portion of an enclosed transmission line. The line is usually a section of rectangular waveguide or coaxial airline. ϵ_r and μ_r are computed from the measurement of the reflected signal S_{11} and transmitted signal S_{21} .

- Free space methods use antennas to focus microwave energy at or through a slab or sheet of material.
- Resonant cavities are high Q structures that resonate at specific frequencies. A piece of sample material inserted into the cavity affects the resonant frequency and quality factor (Q) of the cavity. From these parameters, the complex permittivity of the material can be calculated at a single frequency.
- The parallel plate method, also called the three-terminal method in ASTM standard D15012, involves sandwiching a thin sheet of material or liquid between two electrodes to form a capacitor. The measured capacitance is then used to calculate permittivity. In an actual test setup, two electrodes are configured with a test fixture sandwiching dielectric material. The impedance-measuring instrument would measure vector components of capacitance (C) and dissipation (D) and a software program would calculate permittivity and loss tangent. The method works best for accurate, low frequency measurements of thin sheets or liquids.
- Relative permeability of magnetic material derived from the self-inductance of a cored inductor that has a closed loop, such as the toroid core, is often called effective permeability. The conventional method of measuring effective permeability is to wind some wire around the core and evaluate the inductance with respect to the ends of the wire. This type of measurement is usually performed with an impedance analyzer.

Many factors are involved when it comes to the selection of the measurement method to be used. One can state the frequency range needed for the operation, the required measurement accuracy vis-à-vis time consumption, forms of the materials, temperature, and cost. However, each one of the stated methods has its limitations when it comes to

the needed application in this work [8]. In fact, some of these methods only measure the real part of the permittivity [9], other methods are limited in their capability to measure properties at varying depths in the soil [10], some are not suited for in-situ measurements [11] and still others measure soil parameters at frequencies below 1 GHz.

Theoretically, the Maxwell's equation for a medium characterized by σ , ϵ , and μ , are as follows:

$$\nabla \times E = -\frac{\partial B}{\partial t} = -\mu \frac{\partial H}{\partial t} \quad (1.1)$$

$$\nabla \times H = J + \frac{\partial D}{\partial t} = J_c + \frac{\partial D}{\partial t} = \sigma E + \epsilon \frac{\partial E}{\partial t} \quad (1.2)$$

With defining the complex number of the propagation constant γ as:

$$\gamma = \sqrt{j\omega\mu(\sigma + j\omega\epsilon)} \quad (1.3)$$

or

$$\gamma = \alpha + j\beta \quad (1.4)$$

And thus, the electric field can be solved in terms of α and β as:

$$E_x(z, t) = \begin{cases} A e^{-\alpha z} \cos(\omega t - \beta z + \theta) & \text{for } z > 0 \\ B e^{\alpha z} \cos(\omega t + \beta z + \varphi) & \text{for } z < 0 \end{cases} \quad (1.5)$$

The material parameters can be calculated assuming plane wave propagation [12]. The transmission coefficient is determined by measuring the attenuation and phase shift introduced by a sample placed between two antennas. Multiple reflections, edge effects and mismatches are the main sources of error. The multiple reflections, in particular,

can be minimized if the sample thickness fulfills the -10 dB attenuation criterion. ΔA is the attenuation in the signal between the transmitting and the receiving antennas. It is caused by the loss of energy that the incident wave undergoes as it passes through a layer of material. $\Delta\phi$ denotes the phase shift between the measured angle with the presence of the material, and the phase angle measured in free space with the absence of the material. Having defined the main parameters, the relative complex permittivity can be defined as:

$$\varepsilon' \simeq \left(1 + \frac{\Delta\phi\lambda_0}{360d}\right)^2 \quad (1.6)$$

$$\varepsilon'' \simeq \frac{\Delta A\lambda_0\sqrt{\varepsilon'}}{8.686\pi d} \quad (1.7)$$

However, the stated formulas can be used assuming plane wave propagation in a low loss material [12]. There is no clear definition for an expression to extract the parameters of a material in general types of propagations, which explains the need to develop a new device to do the job.

1.4 Outline

In Chapter 2, a brief description of the monopole and dipole antennas is provided. In addition, the antenna selection for this work is explained.

Chapter 3 presents the finite difference time domain method that will be used throughout the work.

Based on the selected antennas and the FDTD method, Chapter 4 shows the probe design for the different cases of selected antennas.

Chapters 5 shows the measurements done in the lab, and the comparison with the simulated results.

Finally, Chapter 6 concludes with a summary of the main results of the project and suggestions on possible ways to supplement and enhance the work.

CHAPTER 2

Chapter 2 – ANTENNAS AND FDTD METHOD

In this Chapter, the horn and dipole antennas are introduced. In addition, monopole antennas are defined with their major parameters.

2.1 Antennas Theory

Antennas are devices used to radiate electromagnetic waves, resulting from the acceleration of the charges. For the case of a transmission line, the waves in both directions cancel out and radiation will not occur. Whereas by bending the ends of the transmission line, the currents will become parallel, and they will add up to create radiating antennas. Each antenna has its specific form and characteristics, and consequently, its radiation will differ from other types of antennas: this is referred to as the radiation pattern of the antenna. The radiation pattern of the horn antenna specifically is shown in Figure 2.1, and the one of a dipole antenna is shown in Figure 2.2. The horn antenna is more directive than a dipole antenna because it focuses its radiations in one direction and its gain increases to reach 20.48 dB in this direction which is across its aperture. Whereas the dipole antenna's radiation diverges more, leading to more side lobes, and the gain on the side of the antenna decreases to reach 0 dB on the perpendicular side of the dipole antenna's axis. The dipole antenna radiates in all directions except from the direction of its axis.

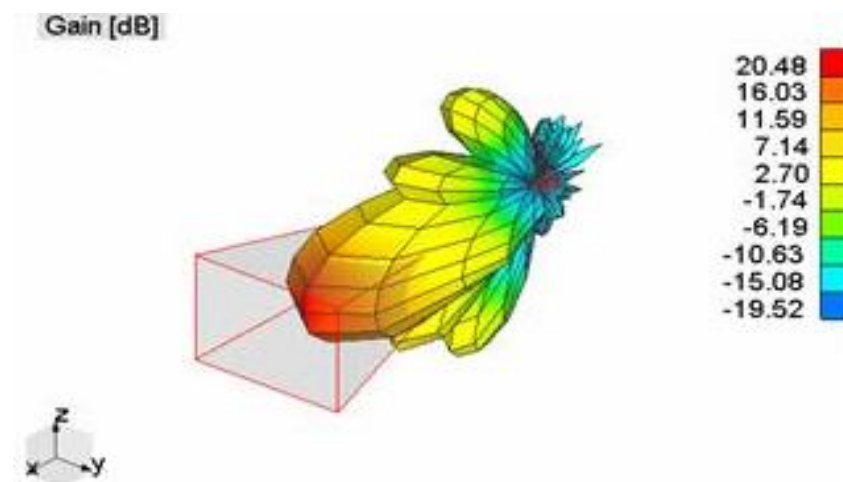


Figure 2.1 - Horn Antenna Radiation Pattern

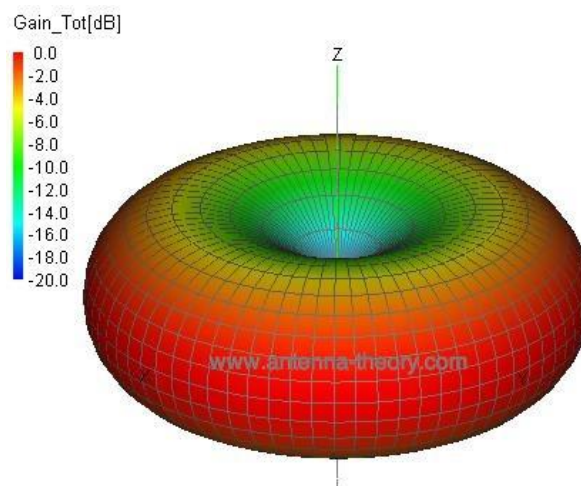


Figure 2.2 - Dipole Antenna Radiation Pattern

2.2 Antenna Selection

Each antenna has its specific form and characteristics, and consequently, it will have its specific parameters. The main parameters to take into consideration when selecting an antenna for a certain application are as follows:

- The radiation pattern will differ from one to another type of antennas. An antenna radiation pattern or antenna pattern is defined as a mathematical

function or a graphical representation of the radiation properties of the antenna as a function of space coordinates.

- A radiation lobe is a portion of the radiation pattern bounded by regions of relatively weak radiation intensity. The main lobe is where the intensity is concentrated. Minor lobes present usually relatively weaker intensities and they are somehow far from the main lobe. Minor lobes usually represent radiation in undesired directions, and they should be minimized. Side lobes are normally the largest of the minor lobes. The side lobes are near the main lobe with a noticeable field intensity, and the back lobes are usually opposed in direction of the main lobe. In most radar systems, low side lobe ratios are very important to minimize false target indications through the side lobes.

When talking about the radiation pattern, it is important to differentiate some specific types. For example, a directional radiator indicates that an antenna is having the property of radiating or receiving more effectively in some directions than in others. Usually the maximum directivity is significantly greater than that of a half-wave dipole. Whereas an Omnidirectional radiator is said to an antenna having an essentially nondirectional pattern in a given plane and a directional pattern in any orthogonal plane. An Isotropic radiator is a hypothetical lossless antenna having equal radiation in all directions.

- The beam width of an antenna is a very important figure of merit and often is used as a trade-off between it and the side lobe level; that is, as the beam width decreases, the side lobe increases and vice versa. The beam width of the antenna is also used to describe the resolution capabilities of the antenna to distinguish between two adjacent radiating sources or radar targets.

- Radiation intensity in a given direction is defined as the power radiated from an antenna per unit solid angle. The radiation intensity is a far-field parameter. It can be obtained by simply multiplying the radiation density by the square of the distance.
- Directivity is the ratio of the radiation intensity in a given direction from the antenna to the radiation intensity averaged over all directions. It is the average radiation intensity is the total power radiated by the antenna divided by 4π . Stated more simply, the directivity of a non-isotropic source is equal to the ratio of its radiation intensity in a given direction over that of an isotropic source.
- The total antenna efficiency e_0 is used to take into account losses at the input terminals and within the structure of the antenna.
- The efficiency of the antenna is given by the multiplication of the reflection or mismatch efficiency, by the conduction efficiency, and the dielectric efficiency.
- The gain of the antenna is closely related to the directivity. It is the ratio of the intensity, in a given direction, to the radiation intensity that would be obtained if the power accepted by the antenna were radiated isotopically.
- Polarization is the curve traced by the end point of the arrow representing the instantaneous electric field. The main types of polarizations are linear, circular and elliptic.

Three types of UWB antennas are used in this work. The first one is a triangular monopole antenna, the second antenna has a circular shape with a ground of two rectangular slots, and the final antenna used is the Deepace antenna, similar to the circular antenna but with a different ground shape.

Monopole antennas currently exist in different sizes and shapes, to respond to various usages and applications. They are available in circular, triangular, square, trapezoidal, and many more geometries. Monopole antennas are usually selected to be introduced in embedded applications requesting an ultra-wide band of frequencies, and when the antenna needs to be attached to another device. This is an advantage of UWB monopole antennas over other types of antennas because of their smaller sizes that can fit into critical applications. The size constraint of monopole antennas was moreover solved with the planar monopole antennas, in which the ground plane of the antenna is no more orthogonal to the antenna plane, but replaced by a coplanar ground plane instead. This way, the occupied volume by the antenna got much smaller and widens the area of application of the antennas in question. The performance of the UWB monopole antennas depends on many factors if one needs to modify the operating frequency for example. From the factors can be selected mainly the tapering the feed region asymmetrically or symmetrically, shorting post which can lower the operating frequency by introducing an additional mode, or increasing the length of the notch or strip lengthens the current path and lowers the operating frequency. Each factor can be studied separately depending on different monopole types, and observations will help to extract the antennas behaviors according to the changes.

A small ultra-wide band planar monopole antenna is the one of interest for this developed project, because of its acceptable size and most commonly directive beam. For this purpose, a qualitative study to observe the physical behaviors of such antennas is conducted here below [13, 14].

Since the antenna to be used has a planar geometry, the current will be concentrated on the edges of the conductors. In the case of a circular disk shaped antenna, the current will flow from the feed to the external edge of the antenna's circle. Hence, the current

path can be approximated as half of the perimeter of the disk, that is $L = \pi R = \frac{1}{2} \pi d$, where R is the radius of the antenna's disk and d is its diameter. The elements of the analyzed antenna are found to resonate at frequencies where their lengths are an odd multiple of $\lambda/4$. Figure 2.3 highlights the frequencies of resonance, noting that the transition from one resonance to the other shows a thin clue on the plot. An additional element to take into consideration when analyzing high frequency performance of the antennas is the feed region. This parameter has high impacts as imperfections in the feed region will affect the high frequency cut-off.

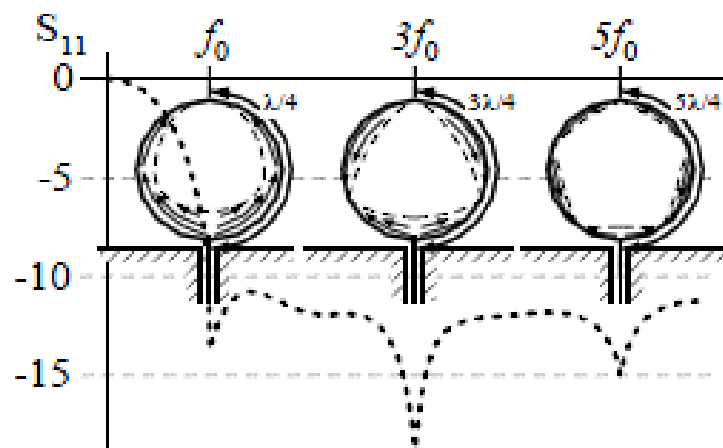


Figure 2.3 - Resonance of Circular UWB Antennas

Another comparison to be examined is the difference in behaviors between spherical, disk and half disk UWB antennas, shown in Figure 2.4 a, 2.4 b and 2.4 c respectively. As shown in the figures, the three antennas have a ground plane of radius 2.54cm. The sphere and the disk have a diameter or height of 2.54 cm while the height of the half disk is 1.27cm as indicated. At a frequency of 3 GHz for example, $\lambda = \frac{c}{f} = 10\text{cm}$. Consequently, the sphere and the disk are having a diameter of $\lambda/4$ almost, so this is the frequency where they will be matched, and the plots in Figure 2.5 prove this

behavior. The fundamental resonance occurs at the effective length found previously as $L = \pi R = 1.27\pi = \lambda/4$, thus $\lambda = 4L = 16\text{cm}$. In this case, the frequency will be $f = \frac{c}{\lambda} = 1.9\text{ GHz}$.

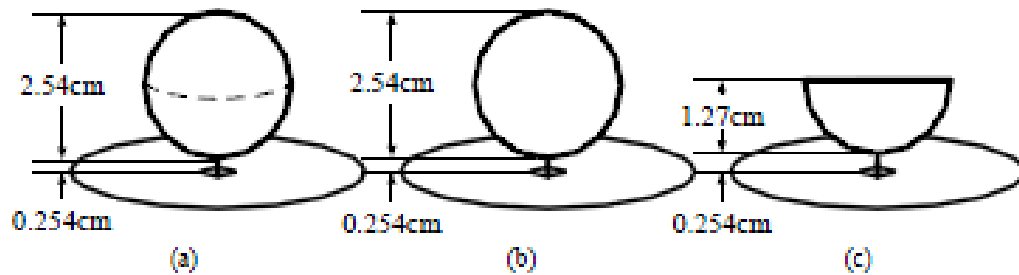


Figure 2.4 - Antennas Geometries

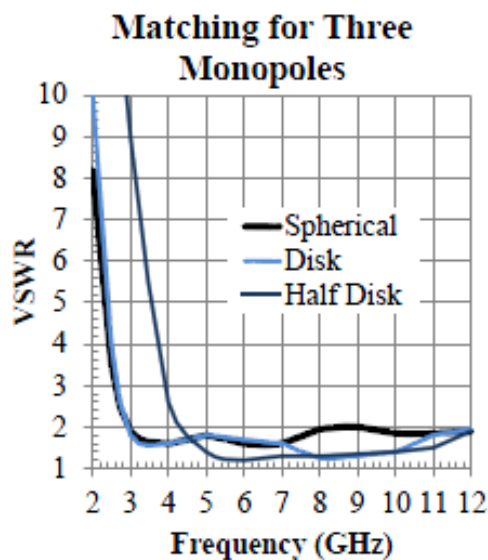


Figure 2.5 - VSWR vs. Frequency

2.3 Theory of FDTD

The studies and implementations were performed using different software, based on the needs and the desired results. The general observations of a propagating wave in different types of soils was performed on XFDTD. Since analytical expressions for the

received signal are not easy to obtain due to the multiple interactions of the antennas with the probe structure and the soil, numerical simulations will be used to provide reference data. This data when compared with measurements can provide the values of the electrical parameters of the soil. The FDTD method [15,16] is used to model the transmitting and receiving antennas at first, and the different types of soil in which it is immersed. FDTD is an efficient method to use when simulating heterogeneous materials over a wide range of frequencies. The software used in this work is the XFDTD program by REMCOM [17]. This software was also used to observe a 3D implementation of waves propagating from the transmitting antenna to the received antenna through the soil type selected. In addition, Matlab software was also used as a backup tool to analyze the obtained results of the FDTD simulations and specify the soil type in question.

As stated, the simulations are done using the XFDTD program. It is a program used to study 3D electromagnetic models, created easily and efficiently following four steps. The first one is defining the geometries used, and second creating the mesh. Some commonly used geometries are predefined in the program, and they can be chosen simply by inserting their dimensions. Third, the run parameters are specified. The most used types of sources are built in the program and can be selected directly, in addition to the ability to modify some of the parameters of the source like the amplitude, pulse width and frequency. Finally, the last step consists of requesting the results of the simulation. The results can be calculations, field snapshots in 2D or 3D plots, and/or movies.

The FDTD method follows is mainly used to solve complicated electromagnetic problems because of its high efficiency when dealing with this type of analysis. This

technique is based on finite differences highlighted in Maxwell's equations. The FDTD method operates in a cyclic manner: The electric field is calculated at a certain time, then the magnetic field will be calculated at the next time. From it, the electric field and the next coming time will be calculated and so on. The FDTD provides 1D 2D and 3D results, and using the specified software, one can observe some animated displays of the propagating field.

2.4 Deriving Equations

The FDTD method employs finite differences as approximations to both the spatial and temporal derivatives that appear in Maxwell's equations. From [7], the central difference approximation, which provides an approximation of the derivative of the function at x_0 , is derived to be

$$\left. \frac{df(x)}{dx} \right|_{x=x_0} \approx \frac{f\left(x_0 + \frac{\delta}{2}\right) - f\left(x_0 - \frac{\delta}{2}\right)}{\delta} \quad (2.1)$$

However, the function is actually sampled at the neighboring points $x_0 + \frac{\delta}{2}$ and $x_0 - \frac{\delta}{2}$.

The FDTD algorithm follows the Yee algorithm which is summarized as replacing all the derivatives in Ampere's and Faraday's laws with finite differences at first. Then, the algorithm goes by solving the resulting difference equations to obtain some update equations that express the new fields in terms of the already known ones. The next step is evaluating the magnetic fields one time-step into the future so they are now known and become the already known fields. Same goes for the electrical fields and so on until the needed fields at the needed fields are known. The 1-dimensional implementation of the described algorithm is shown in Figure 2.6.

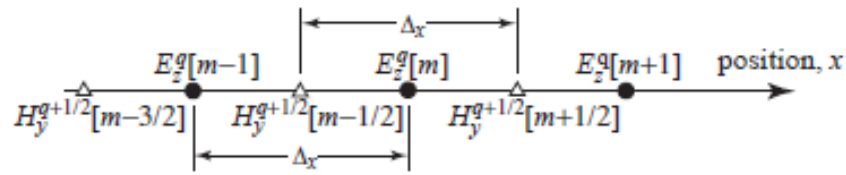


Figure 2.6 – 1D FDTD Implementation

Considering a 1-dimensional varying fields to be calculates using the finite difference time domain method. Assuming that the fields are varying along the x direction, Faraday's law and Ampere's law equations can be written as follows

$$-\mu \frac{\theta H}{\theta t} = \nabla_x E = \begin{vmatrix} \hat{a}_x & \hat{a}_y & \hat{a}_z \\ \frac{\theta}{\theta x} & 0 & 0 \\ 0 & 0 & E_z \end{vmatrix} = -\hat{a}_y \frac{\theta E_z}{\theta x} \quad (2.2)$$

$$\varepsilon \frac{\theta E}{\theta t} = \nabla_x H = \begin{vmatrix} \hat{a}_x & \hat{a}_y & \hat{a}_z \\ \frac{\theta}{\theta x} & 0 & 0 \\ 0 & H_y & 0 \end{vmatrix} = \hat{a}_z \frac{\theta H_y}{\theta x} \quad (2.3)$$

$$\mu \frac{\theta H_y}{\theta t} = \frac{\theta E_x}{\theta x} \quad (2.4)$$

$$\varepsilon \frac{\theta E_z}{\theta t} = \frac{\theta H_y}{\theta x} \quad (2.5)$$

Following the derivations done in [7], a one step ahead in space of the magnetic field, and a one step ahead in space of electric field were found to be as follows:

$$H_y^{q+\frac{1}{2}} \left[m + \frac{1}{2} \right] = H_y^{q-\frac{1}{2}} \left[m + \frac{1}{2} \right] + \frac{\Delta t}{\mu \Delta x} (E_z^q[m+1] - E_z^q[m]) \quad (2.6)$$

$$E_z^{q+1}[m] = E_z^q[m] + \frac{\Delta t}{\epsilon \Delta x} (H_y^{q+\frac{1}{2}}[m + \frac{1}{2}] - H_y^{q+\frac{1}{2}}[m - \frac{1}{2}]) \quad (2.6)$$

Similarly, the 3-dimensional FDTD can be explored using the same approach, except that the field will be defined using 3 indices x, y and z. Figure 2.7 shows the three indices of the electric field and Figure 2.8 shows the Yee cube arrangement of nodes in a 3 dimensions system.

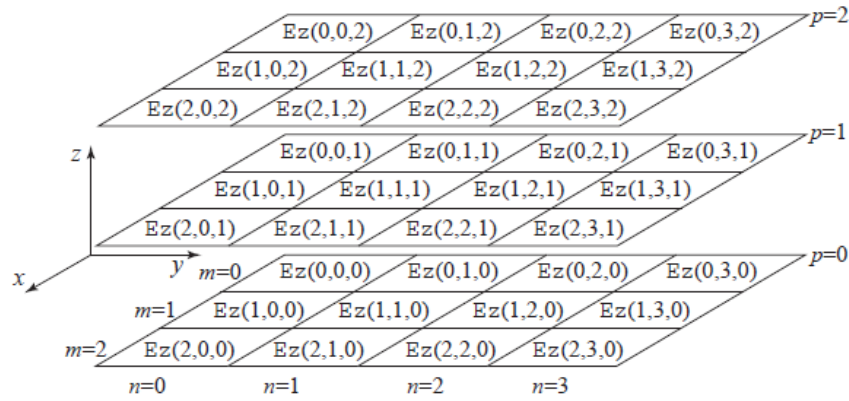


Figure 2.7 – 3D indices of Electric Field

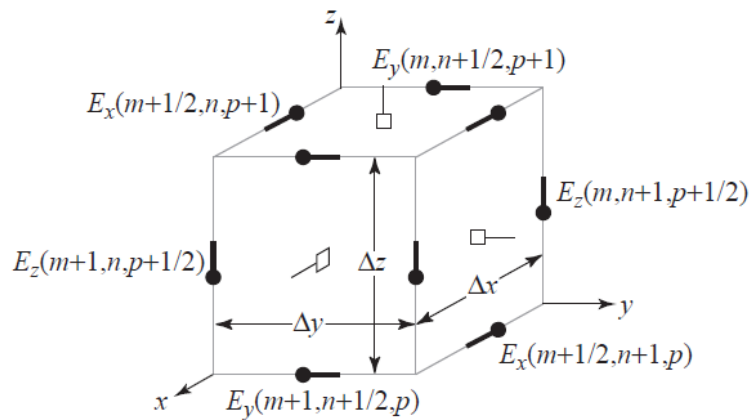


Figure 2.8 - Yee Cell in 3D System

CHAPTER 3

Chapter 3 - PROBE DESIGN

In this Chapter, the different antennas used in the probes will be presented. First, the triangular monopole antennas will be integrated in the probe and tested. Next, circular monopole antennas will replace the triangular monopole antennas for wider frequencies of operation. Next, the planar dipole antennas, Deepace antennas will be modeled in the third section.

3.1 Design Block Diagram

The new design to be developed in this work will be based on the principle of measuring the changes in the amplitude and phase of the wave in the soil in question in order to find its electrical parameters. The advantage of this technique is that the measurements can be done in situ, in order to maintain the properties of the soil without any extraction or modification. In addition, the soil samples shall be assumed to be non-ferromagnetic. Figure 3.1 shows the sketch of the block diagram to be implemented.

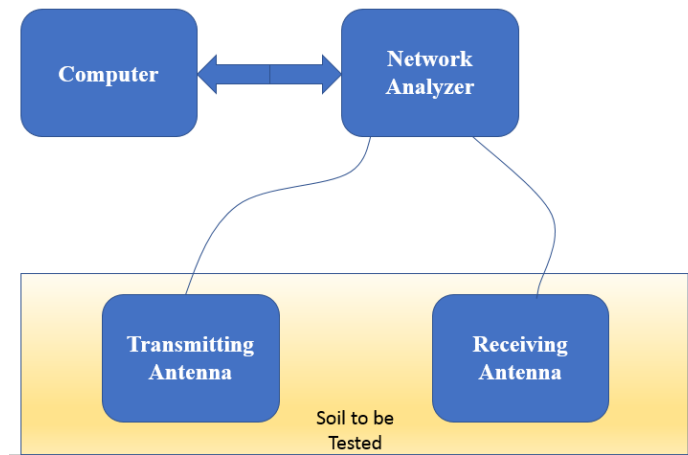


Figure 3.1 - Design Sketch

As per the design sketch shown, a signal will be generated by the network analyzer which is controlled by a computer and transmitted by one antenna. The other antenna will receive the signal. The sample procedure is done in air and in soil in order to calibrate for cable and reflection losses. While implementing the design, essential parameters will be defined, including the frequency, the transmitting and receiving antennas' structures and the distance between the two antennas.

The probe is portable and well-suited for in-situ measurements in conjunction with portable wideband Vector Network Analyzers (VNAs) currently available in the market. The VNA is connected to a personal computer which maps the measured values of the transmission coefficient to pre-calculated values obtained from 3D numerical simulations of the probe when immersed in different types of soil.

The two antennas are placed at a distance of 10cm. The antennas should be protected by a plexi cover, and the coaxial cables should be protected by 2 metallic

cylinders that penetrate in the ground. A detailed sketch is shown in Figure 3.2.

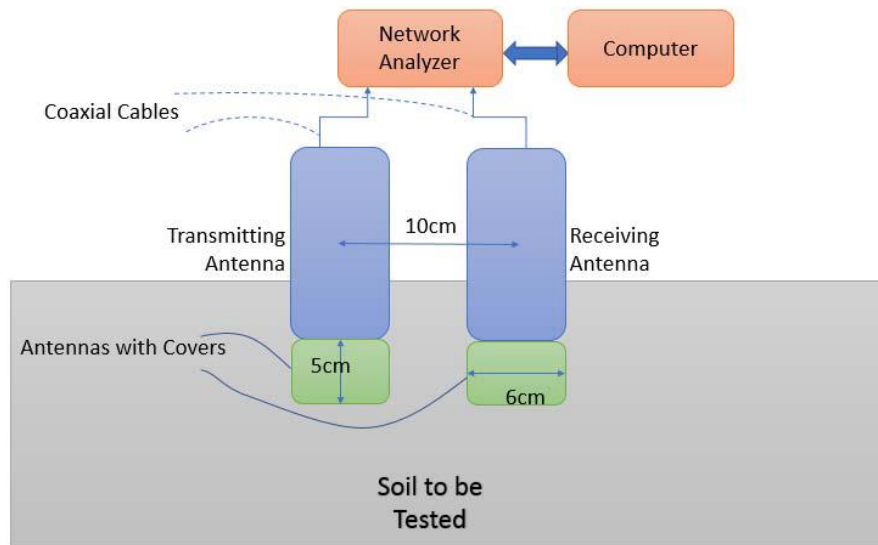


Figure 3.2 – Detailed Design

3.2 Triangular Monopole Antennas

3.2.1 Building the Geometry

This part consists of defining the different geometries used, including the transmitting and receiving antennas, their plexi covers and steel cylinders. The first step was to define a rectangular box, to be used as the medium in which the antennas are placed. The source used is a differentiated Gaussian pulse (DGP), it is located at the base of the monopole antenna just above the ground plane. A plot of the DGP is shown in Figure 3.3, and its frequency spectrum is shown in Figure 3.4. The receiving monopole antenna was defined as a passive component where the received signal is computed.

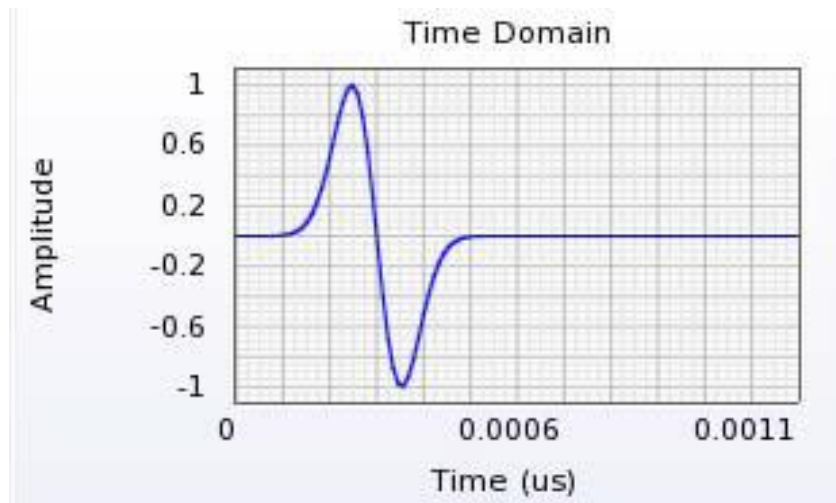


Figure 3.3 - Plot of DGP vs. Time

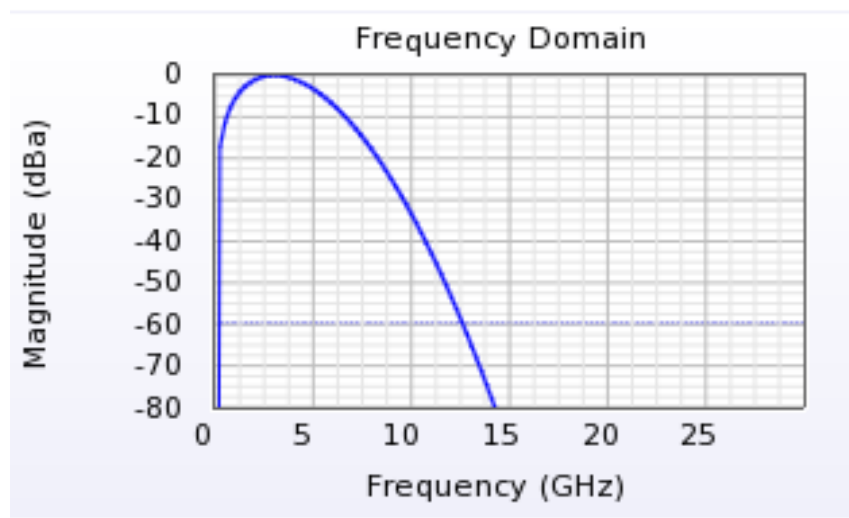


Figure 3.4 - Plot of DGP vs. frequency

At first the medium was defined to be as free space, and the material type of this box was changed continuously by going further into the analysis.

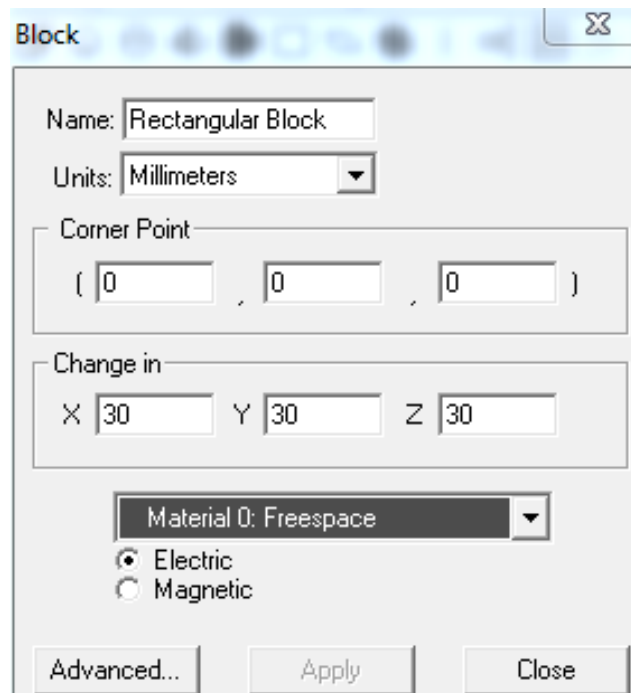


Figure 3.5 - Rectangular Medium

Next, the two wires were defined, to play the role of the monopole transmitting antenna and receiving antenna. In addition, a ground disk was defined, made of a perfect electric conductor material. The antennas were connected using a coaxial cable, defined by a dielectric material separating the two conductors. In addition, two steel or aluminum cylinders were introduced to cover the coaxial cable from above. Finally, in order to protect the antennas entering the soil structure, a cover was defined to be made of a plastic material. The described geometry construction is illustrated in Figure 3.6.

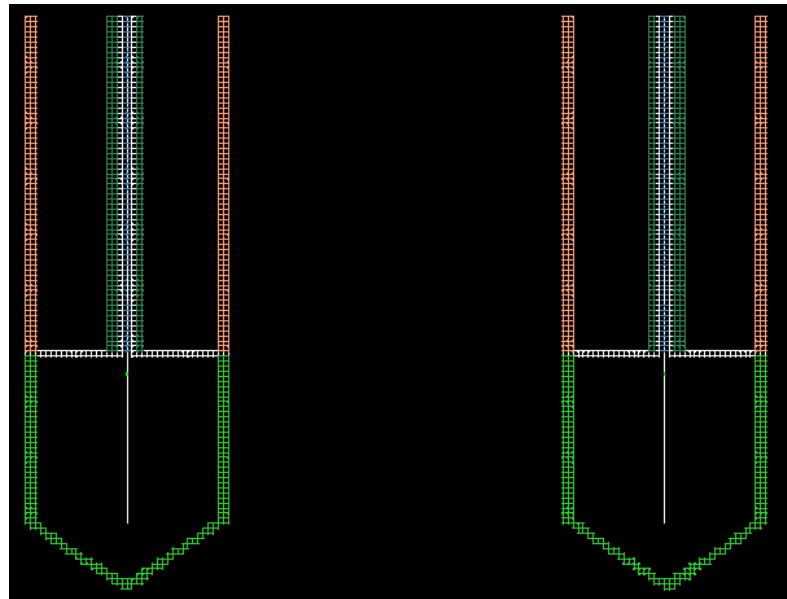


Figure 3.6 - Complete Geometry

However, when running the simulations for the current geometry, the obtained S_{11} showed that the antenna used was very narrow banded, which makes it unsuitable for the needed application. For this purpose, the monopole antenna was aimed to be wide-band; therefore a triangular shaped monopole was inserted as shown in Figure 3.7. Different materials were defined in order to construct the above geometry. For example, the dielectric used in the coaxial cable was defined to have a permittivity of 2.25 and a conductivity of 0. The plexi glass covers have a permittivity of 3.2 and a conductivity $1e-19S/m$. The aluminum cylinder has a permittivity of 1.7 and a conductivity of $3.8e7S/m$.

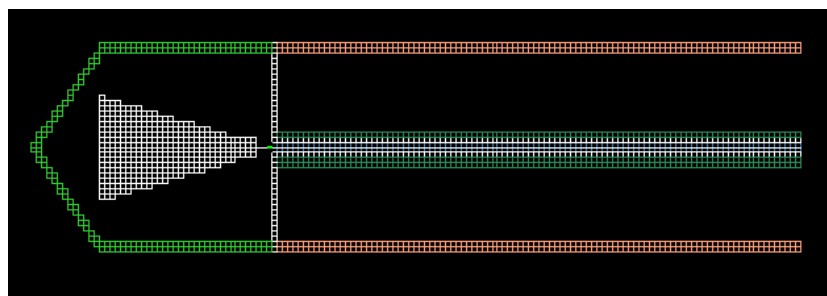


Figure 3.7 - Triangular Monopole Antenna

3.2.2 Defining the Signal

In this step, the source was defined to be a differentiated Gaussian Pulse. DGP will travel through the slab, from the transmitting antenna to reach the receiving one. For this purpose, an active source is defined on the transmitting antenna, and load is defined on the receiving antenna facing the active source. This is shown in Figure 3.8.

#	Port	Type	(Amp/Phase)	Dir.(X,Y,Z)	Load/Switch Type	(R,L,C) or Switch Params (Time step,Duration)
1	Y	Voltage	(10.00/0.00)	Z,(88,68,83)	N/A	(5.00e+001,N,N)
2	Y	Passive	N/A	Z,(88,174,83)	N/A	(5.00e+001,N,N)

Figure 3.8 - Source Definition

When the active and load sources are defined, they are marked on the geometry by a green dot to indicate their presence at the defined location.

3.2.3 Requesting the Results

After making sure that the geometry is well built and the sources are defined, the simulation was run and the results were requested; in this case, the field at the receiving antenna was recorded at several time steps in order to get a full movie that can be generated and illustrates the wave propagation. Also the field can be plotted at the transmitting and receiving antennas versus time. In frequency domain, some main parameters can be plotted, such as the impedance, S_{21} in phase and magnitude and the S_{11} magnitude.

The first set of results were obtained with the monopole antenna placed in free space. The transmitted field is shown in Figure 3.9 and the received field was plot in Figure 3.10.

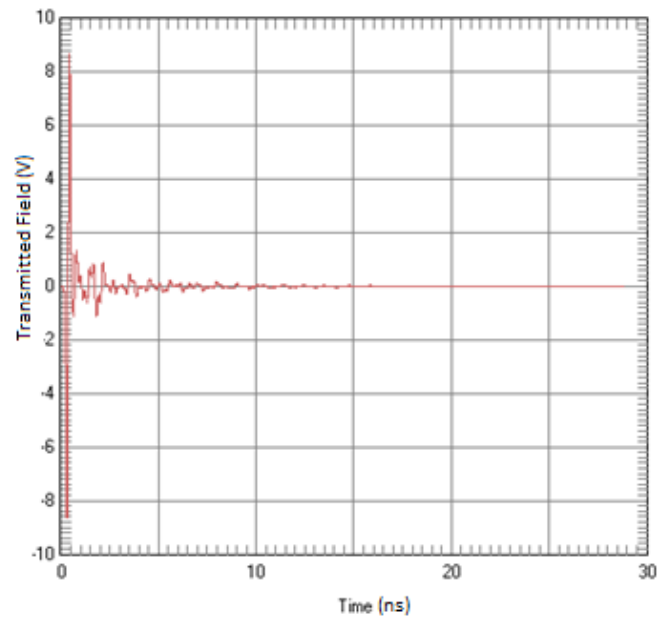


Figure 3.9 – Transmitted Field vs. Time

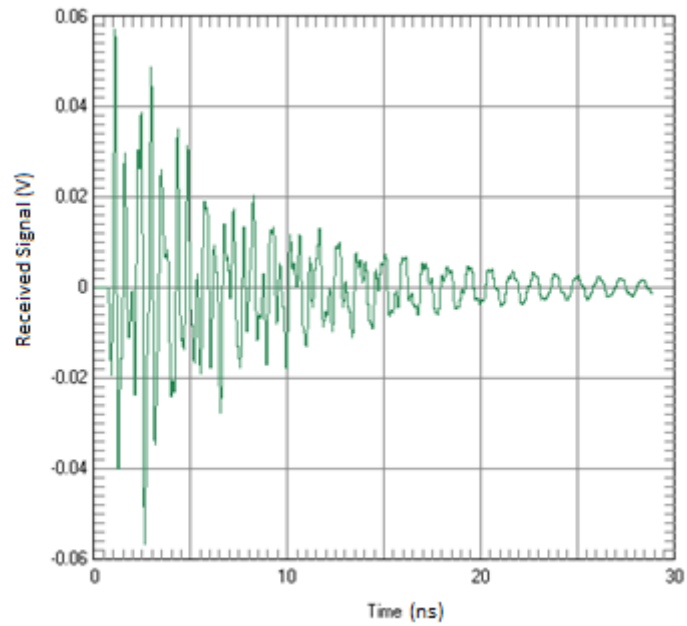


Figure 3.10 - Received Signal in Free Space

In addition, the plot of the magnitude of S_{21} versus frequency is shown in Figure 3.11 below. It should be noted that based on the cell size selected in the model, the results for frequencies above 9 GHz shall not be considered reliable.

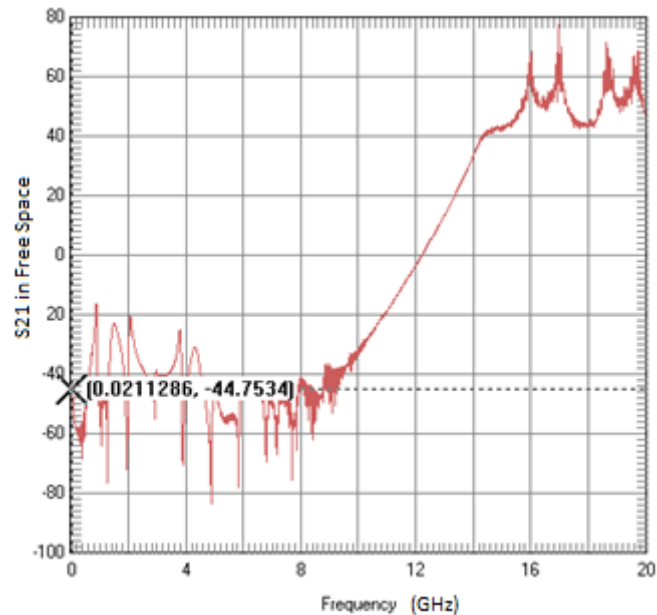


Figure 3.11 - S_{21} in Free Space

Next, the medium was changed to be of soil type 1, defined by having a permittivity of 3. The same results were requested and the received signal and S_{21} are shown in Figures 3.12 and 3.13 respectively.

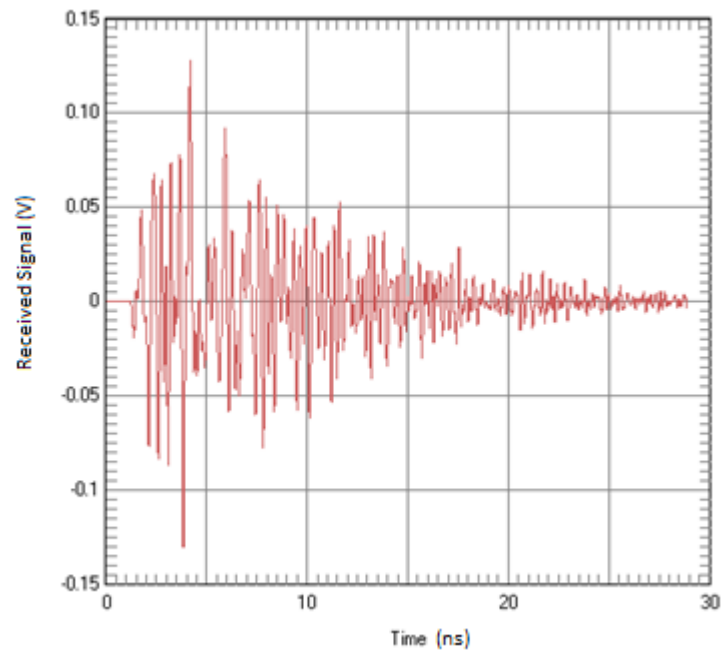
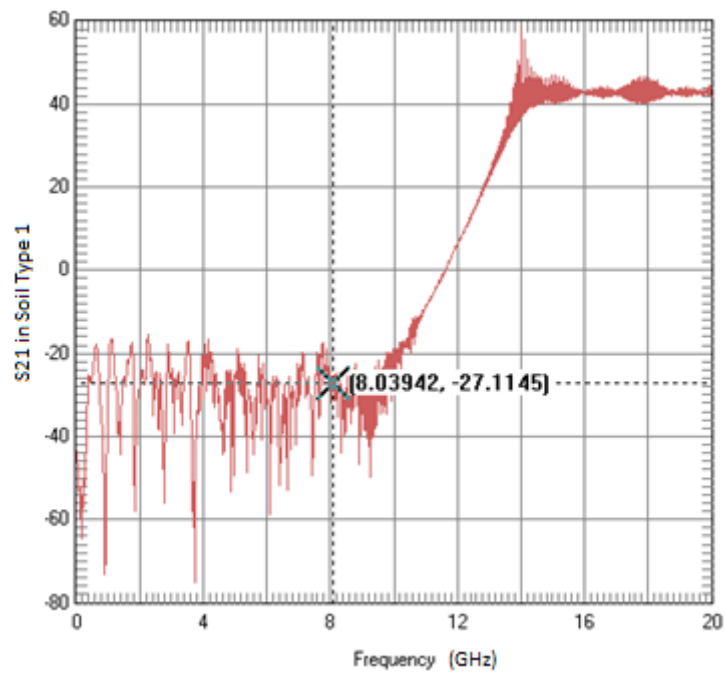


Figure 3.12 - Received Signal in Soil Type 1

Figure 3.13 - S₂₁ in Soil Type 1

Finally, the same results were requested for a second type of soil having a permittivity of 4. The corresponding received signal and S_{21} are shown in Figures 3.14 and 3.15 respectively.

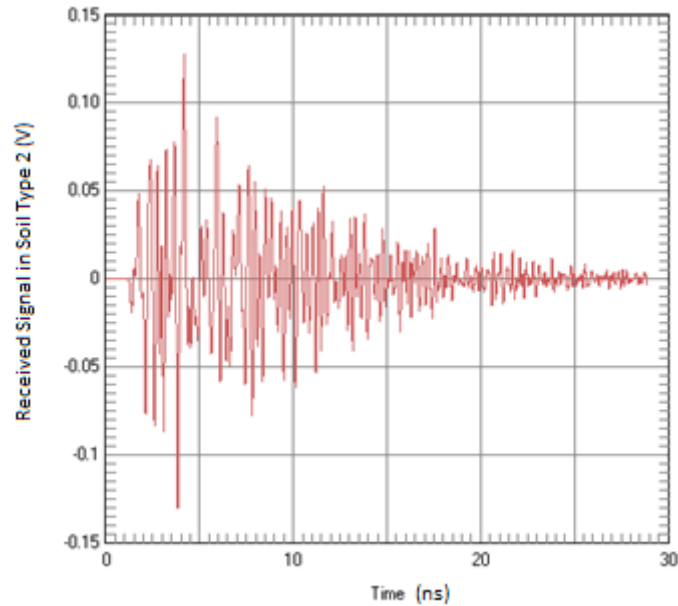


Figure 3.14 - Received Signal in Soil Type 2

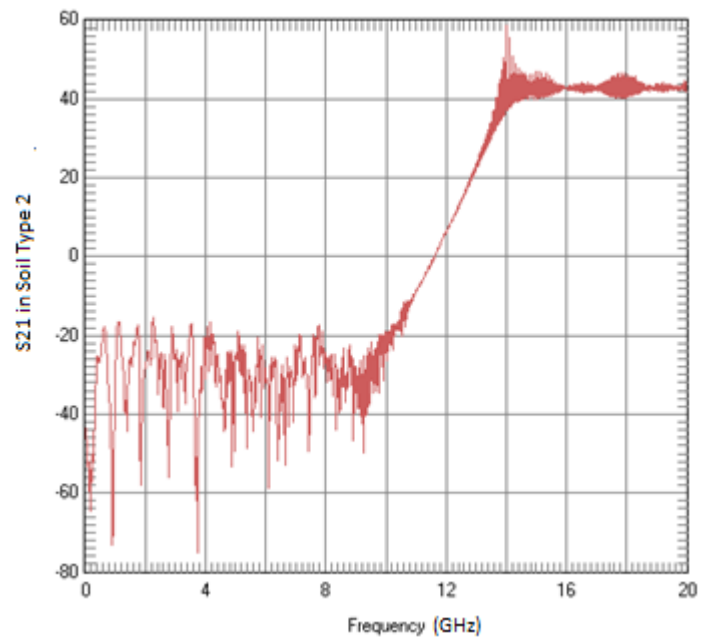


Figure 3.15 - S_{21} in Soil Type 2

3.2.4 Extraction and Processing of the Results using MATLAB

In order to see the results clearer, Matlab software was used to plot the same parameter in different types of soil on the same plot with the free space plots. For this purpose, the data files of each simulation were extracted and inserted into Matlab as matrices. The first tested soil was defined to have a permittivity of $\epsilon_r=3$ and a conductivity of $\sigma=1\text{mS/m}$. Soil type 2 was defined with a permittivity of $\epsilon_r=4$ and a null conductivity $\sigma=0\text{mS/m}$. The third soil type was used to show major difference, so it was defined with $\epsilon_r=10$ and $\sigma=10\text{S/m}$. All three soil types were compared with free space plots for the parameters of interest.

To start with, the magnitude of S_{11} was examined, to make sure it has values between 0 and -30dB. The result of the plots for all soils' cases is shown in Figure 3.16. Next, the magnitude of S_{21} versus frequency was plotted, to check the effect of the permittivity on the values. The result is shown in Figure 3.17. Finally, the phase values of S_{21} , which are affected by the value of the conductivity of the soil, is shown in Figure 3.18.

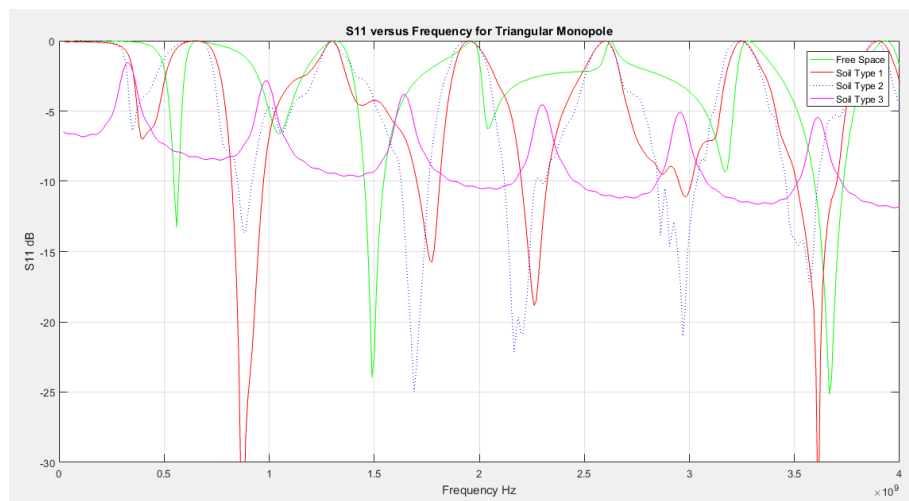
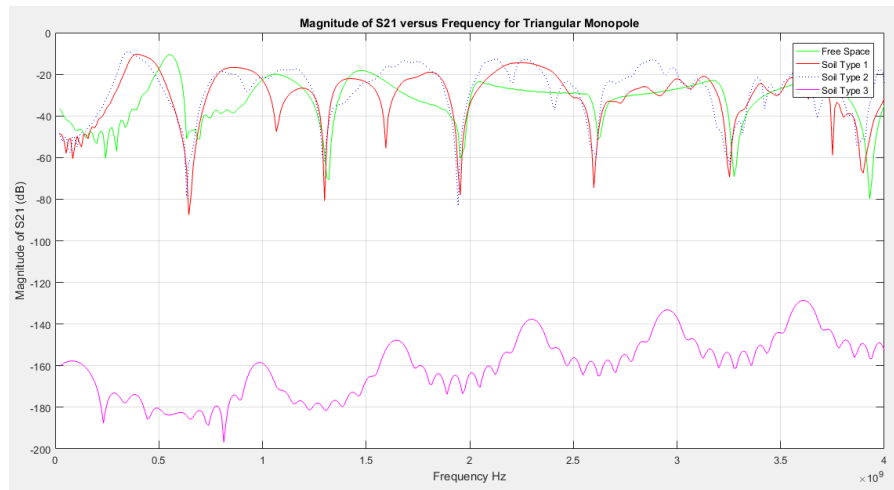
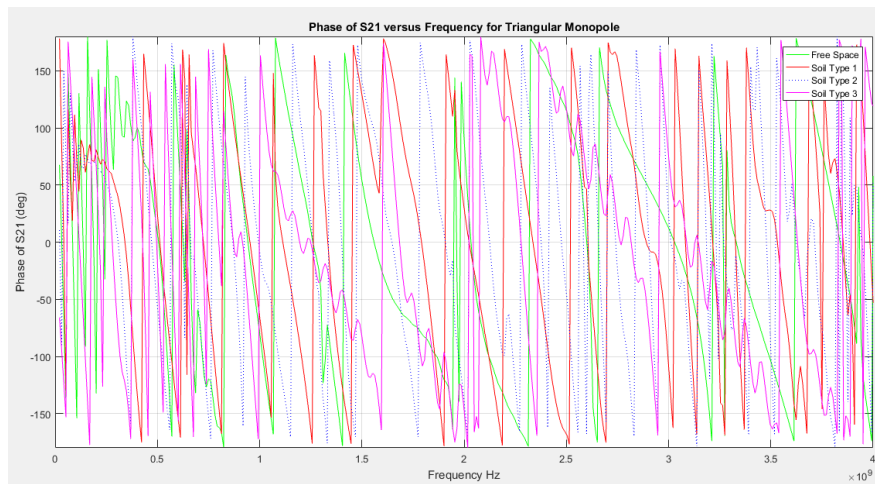


Figure 3.16 - S_{11} vs. Frequency

Figure 3.17 - S_{21} Magnitude vs. FrequencyFigure 3.18 - S_{21} Phase vs. FrequencyTable 3.1 - Comparison of S_{21}

Soil	S_{21} Magnitude at 2 GHz	S_{21} Phase at 2 GHz
Free Space	-29.65588	68.314
Soil Type 1 $\epsilon_r=3$ $\sigma=1\text{mS/m}$	-32.7	20.074
Soil Type 2 $\epsilon_r=4$ $\sigma=0\text{mS/m}$	-26.614	-152.166
Soil Type 3 $\epsilon_r=10$ $\sigma=10\text{S/m}$	-163.28	-160.457

As shown in Table 3.1 above, it is clear that the values of S_{21} magnitudes and phase vary between different types of soil. Accordingly, many simulations can be done in order to extract the changes observed in each case knowing the characteristics of the soil placed. This way, a database can be constructed and used in the developed device to be able to find the characteristics of the tested soil.

3.3 Circular Monopole Antenna

As shown previously is Figure 4.14, the triangular monopole antenna's S_{11} did not exhibit a wideband behavior as required. In fact, S_{11} 's value went lower than 10dB for specific frequencies and not for a large wideband, which makes the antennas behavior somehow critical and maybe unreliable for some frequencies of interest. Hence, another type of antennas was selected for the purpose of getting wider bandwidths. The FDTD model of the two antennas used in this section is shown in Figures 3.19 and 3.20. It is a circular monopole antenna having a rectangular customized ground plane. The FDTD model of the transmitting monopole antenna, the dielectric slab representing the ground in which the antennas are placed, and the receiving monopole antenna are shown in Figure 3.21. The transmitting and receiving antennas are placed facing each other in order to insure maximum reception amplitude.

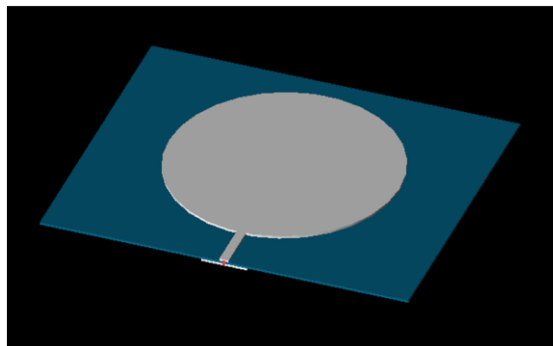


Figure 3.19 - Circular Monopole Antenna - Front View

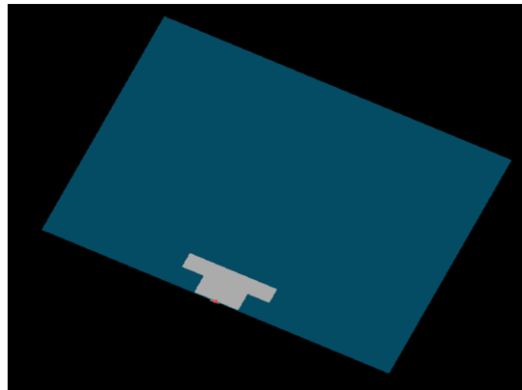


Figure 3.20 - Circular Monopole Antenna - Back View

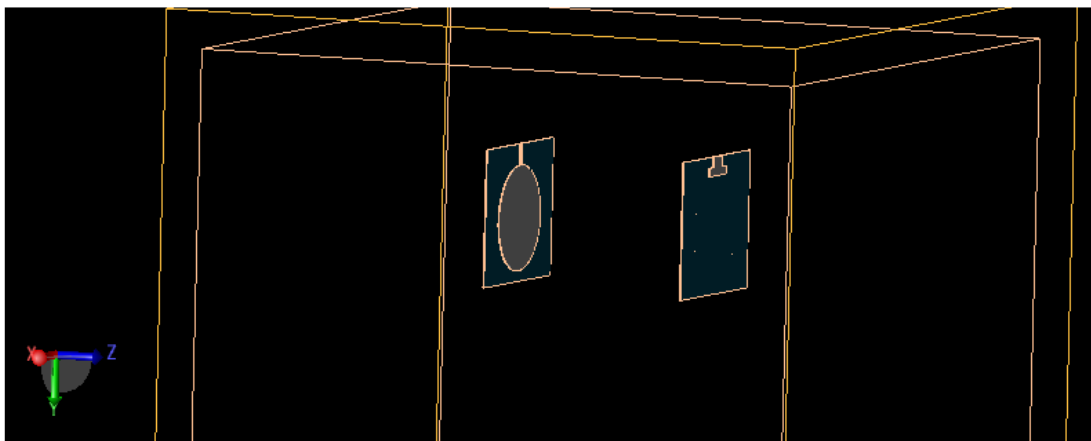


Figure 3.21 - Design Geometry

The FDTD mesh has a size of 30x30x30cm. The grid base cell was generated automatically by the software, in a way to ensure smoothness at the curved edges of the circular antenna.

Several parameters are extracted from the simulation results, such as the antenna impedance (S_{11}), and the received signal (S_{21}). The first simulation was performed with the probe in free space. Then, the material was changed to a soil type 1 (dielectric constant= 3 and conductivity=1mS/m) then soil type 2 (dielectric constant=4 and conductivity= 0 S/m), and soil type 3 (dielectric constant= 10 and conductivity = 1S/m).

Figures 3.22, 3.23 and 3.24 show for the free space case, the transmitted signal versus time, the received signal versus time, and S_{21} magnitude versus frequency respectively.

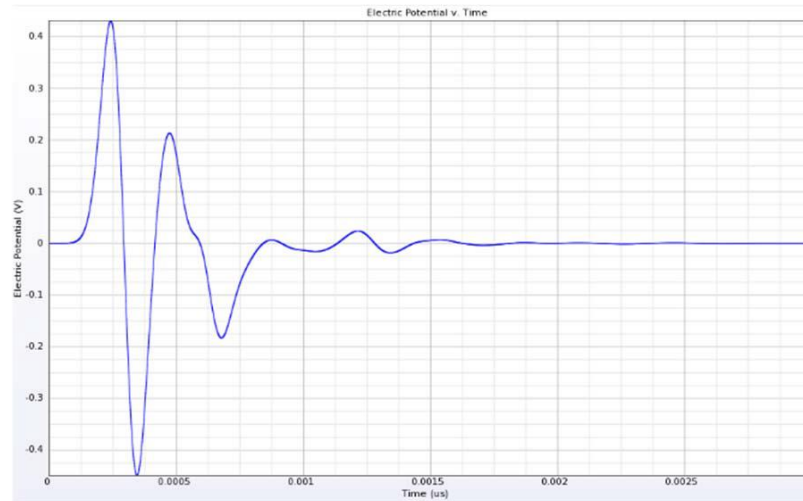


Figure 3.22 - Transmitted Signal vs. Time in Free Space

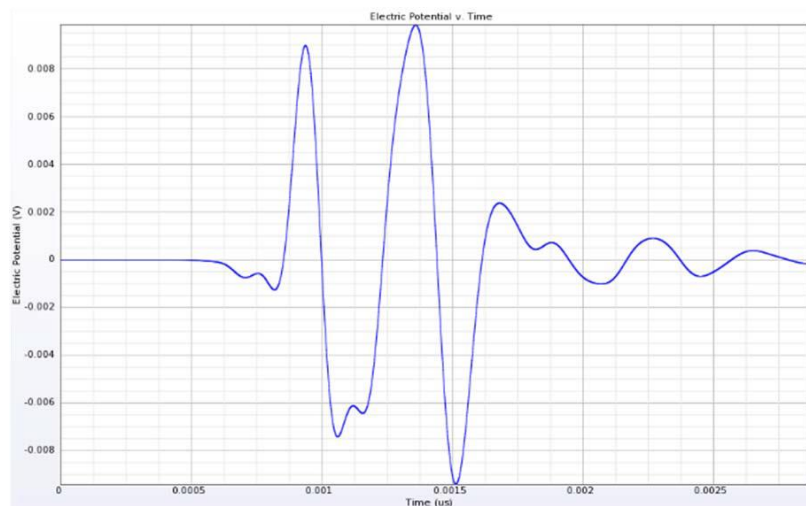


Figure 3.23 - Received Signal vs. Time in Free Space

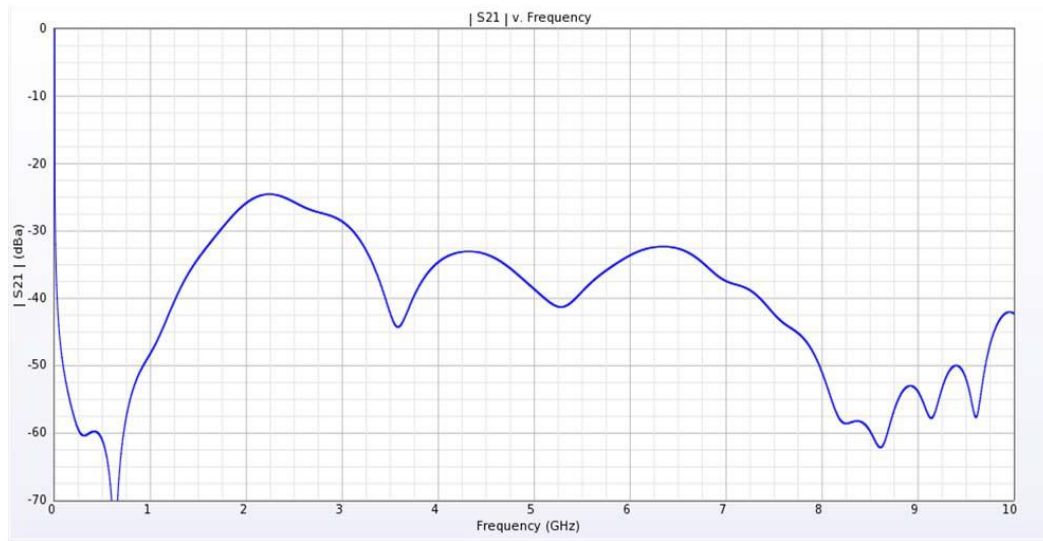


Figure 3.24 - S_{21} Magnitude vs. Frequency in Free Space

Figure 3.25 shows the S_{11} of the antenna used, in free space. Figures 3.26, 3.27, and 3.28 show three different snapshots of the field propagation between the transmitting and receiving antennas, for three consecutive periods of time.

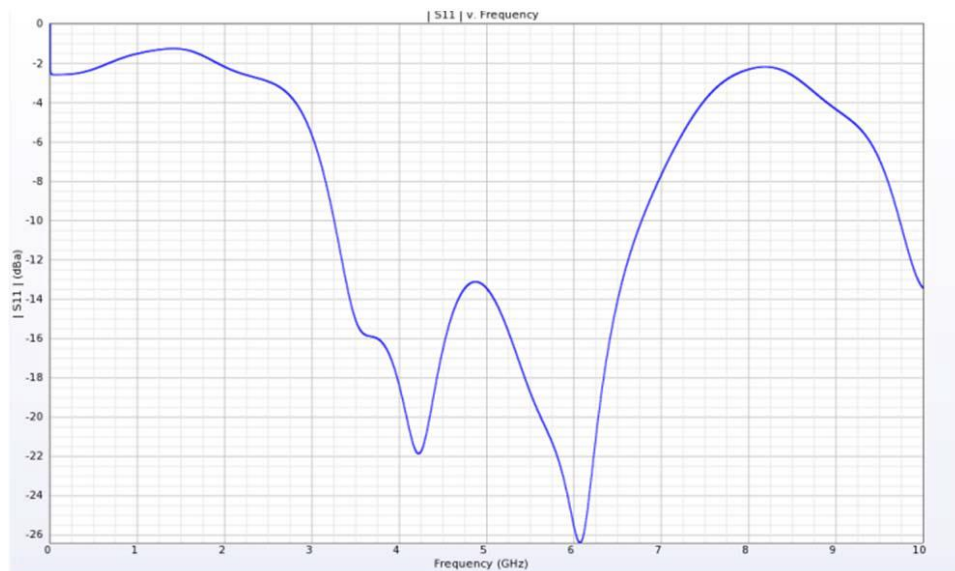


Figure 3.25 - S_{11} vs. Frequency in Free Space

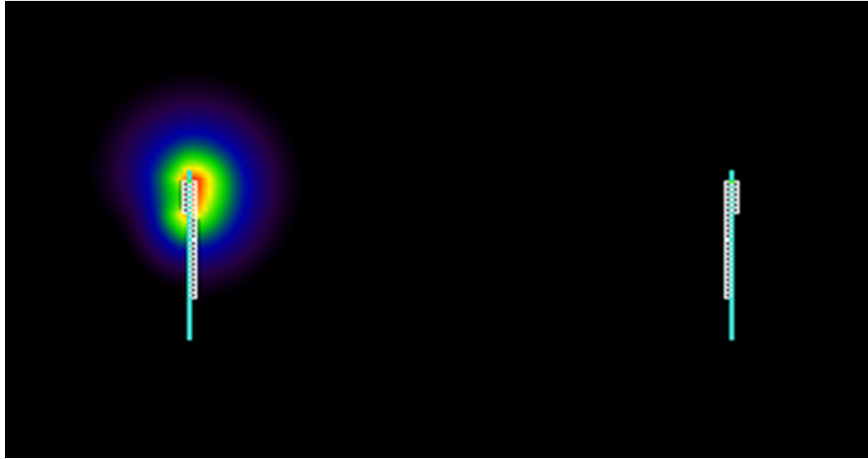


Figure 3.26 - First Snapshot of the Field Propagation in Free Space

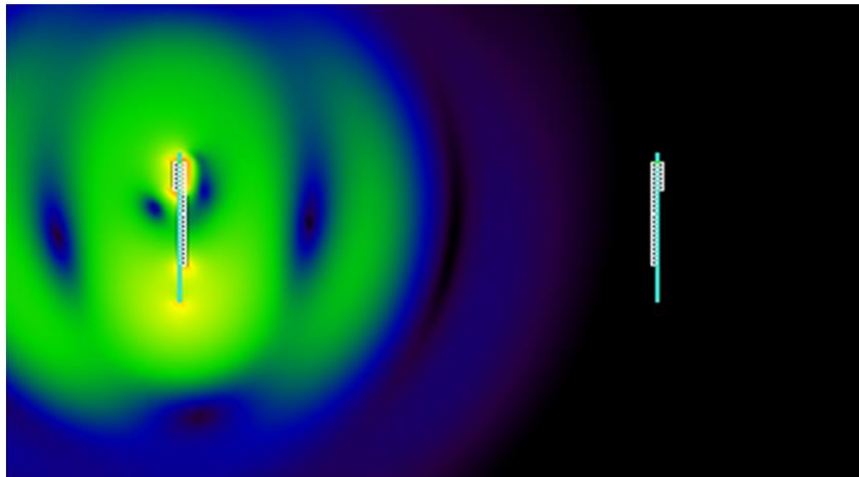


Figure 3.27 - Second Snapshot of the Field Propagation in Free Space

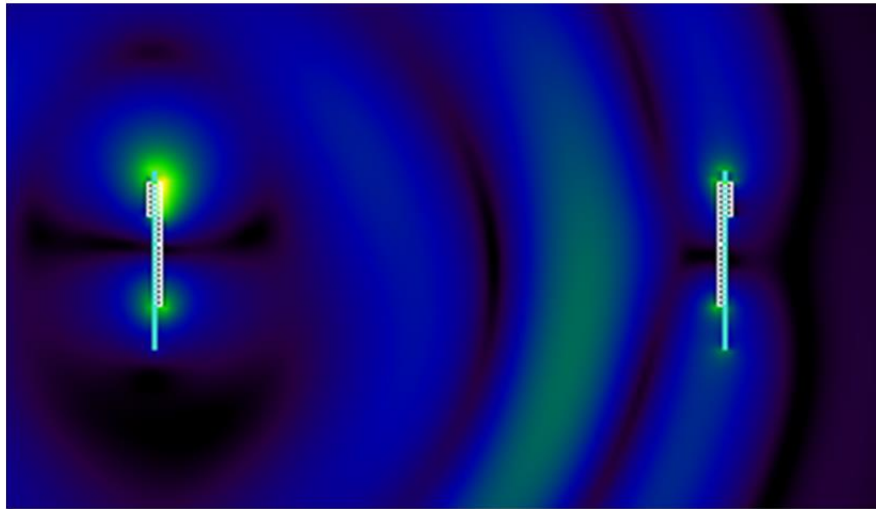


Figure 3.28 - Third Snapshot of the Field Propagation in Free Space

In addition, the 2D radiation pattern of the antenna was extracted at the constant plane of phi being 90° , it is shown in Figure 3.29. Similarly, the 2D radiation pattern of the antenna at constant phi of 0° is shown in Figure 3.30. Finally, the 3D pattern of the antenna is also shown in Figure 3.31.

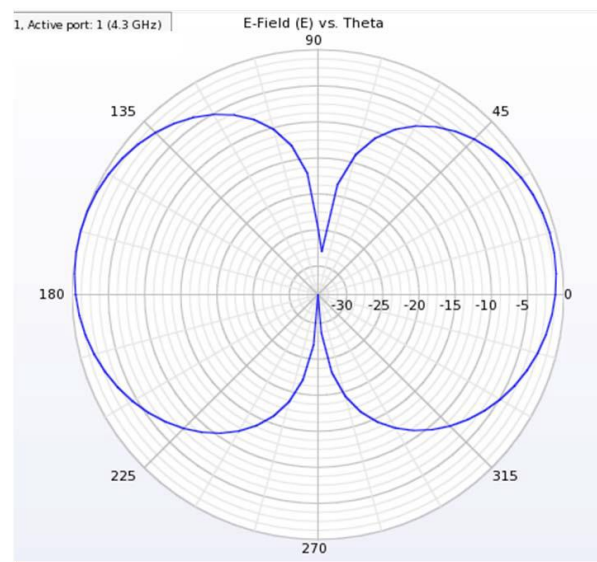


Figure 3.29 - 2D Pattern - Constant Phi 90 Plane

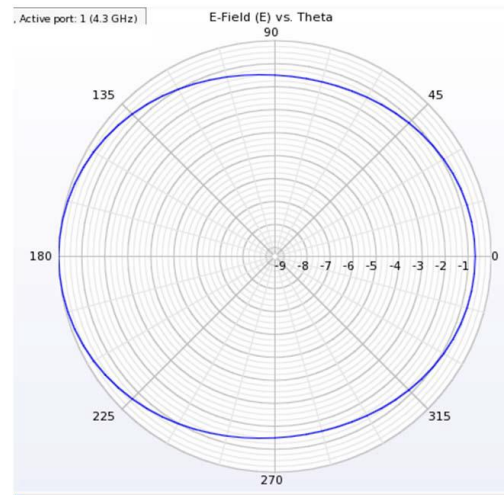


Figure 3.30 - 2D Pattern - Constant Phi 0 Plane

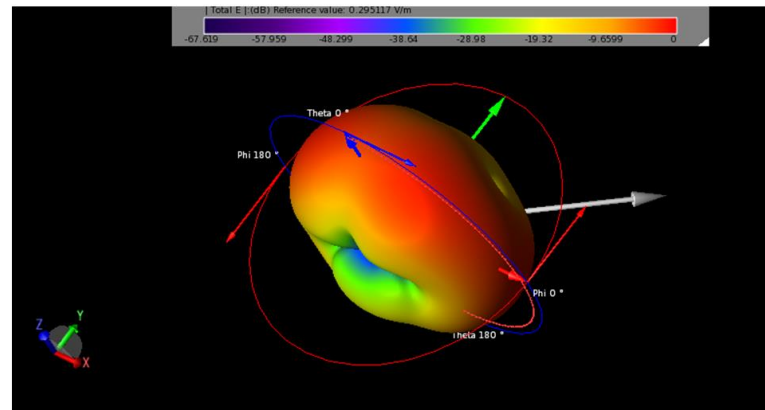


Figure 3.31 - 3D Pattern

Accordingly, the values of S_{21} magnitude and phase were extracted at two different frequencies. The results are shown below.

Table 3.2 - Comparison of S_{21} at 4 GHz

Soil	S_{21} Magnitude at 4 GHz (dB)	S_{21} Phase at 4 GHz (Degrees)
Soil Type 1, $\epsilon_r=3$, $\sigma=1\text{mS/m}$	-77.7	114.25
Soil Type 2, $\epsilon_r=4$, $\sigma=0\text{S/m}$	-95.95	-121.26
Soil Type 3, $\epsilon_r=3$, $\sigma=0\text{S/m}$	-79.53	-108.37

Table 3.3 - Comparison of S_{21} at 5 GHz

Soil	S_{21} Magnitude at 5 GHz (dB)	S_{21} Phase at 5 GHz (Degrees)
Soil Type 1, $\epsilon_r=3$, $\sigma=1\text{mS/m}$	-63.33	-158.48
Soil Type 2, $\epsilon_r=4$, $\sigma=0\text{S/m}$	-67.14	5.24
Soil Type 3, $\epsilon_r=3$, $\sigma=0\text{S/m}$	-64.21	-42.84

As shown in Tables 3.2 and 3.3, at a frequency of 4 and 5 GHz respectively, it is clear that the values of the S_{21} magnitude and phase vary between different types of soil. Accordingly, many simulations can be done in order to extract the changes observed in each case knowing the characteristics of the soil placed. This way, a database can be constructed and used in the field in conjunction with the probe to determine the soil parameters in-situ.

3.4 Planar Dipole Antenna

3.4.1 Theoretical

The circular antenna used in the previous section had a bandwidth of frequencies between 3.2 GHz and 6.7 GHz, based on its S_{11} plot that shows the operation range of the selected antenna. However, in order to enhance the performance of the used antenna, another type was selected, which is the Deepace uwb-2 antenna. It is a unipolar ultra-wide band omnidirectional antenna operating between 2.8 and 11 GHz. This type of antennas is mainly used for ultra-wide band positioning, target sensor data collection, precision locating and tracking applications.

The planar dipole antenna was selected in this section due to its ultrawide band of frequencies of operation. This antenna is affordable and available in the market, it is considered relatively cheap, without compromising on the quality or performance. A prototype of a bottom fed planar elliptical UWB antenna was analyzed [18], for the purpose to check for the major specifications and frequencies of operation. Figure 3.32 shows the parts of the prototype, mainly composed of:

- A coaxial feed line used to deliver the signal pulse to the base of the antenna
- A Balun transformer for the purpose of avoiding spurious currents that cause distortions, and insure the 50Ω matching impedance
- A slot line that guides the energy to the top radiating element

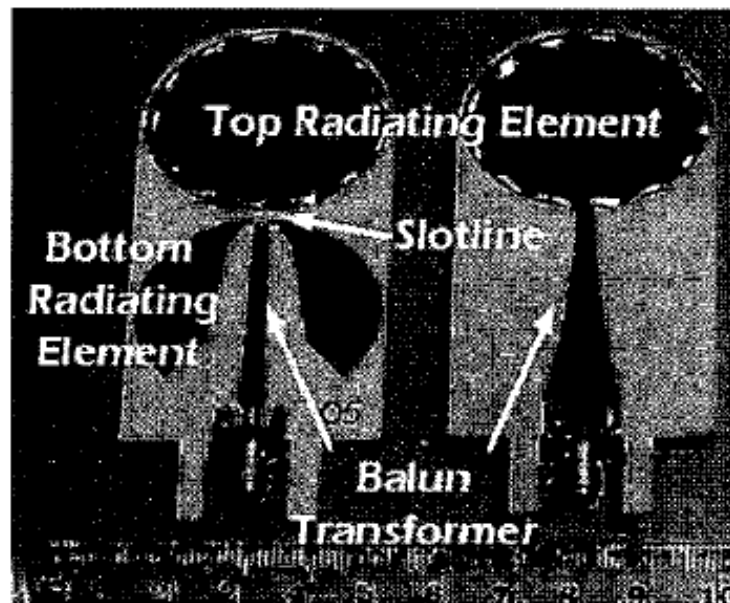


Figure 3.32 - Planar Elliptical Dipole Antenna

The main characteristic of this type of antenna are [18]:

- The antenna is linearly polarized
- It has a VSWR of 1.5:1 and the magnitude of S_{11} is shown in Figure 4.35.
- The antenna's gain is almost 3 dBi

- Its phase response is linear
- This antenna has an efficiency above 90%

The Deepace antenna used in this section is shown in Figure 3.33, and its ground plane is shown in Figure 3.34. As per its datasheet, this antenna has the S_{11} shown in Figure 3.35, which shows that the antenna operation up to 9 GHz. Deepace antenna has also the following specifications:

- 50 Ω impedance
- Power capacity: 5W
- Echo loss: 10dB
- Gain: 3.8dBi
- Size: 30mm*42mm



Figure 3.33 - Deepace Antenna

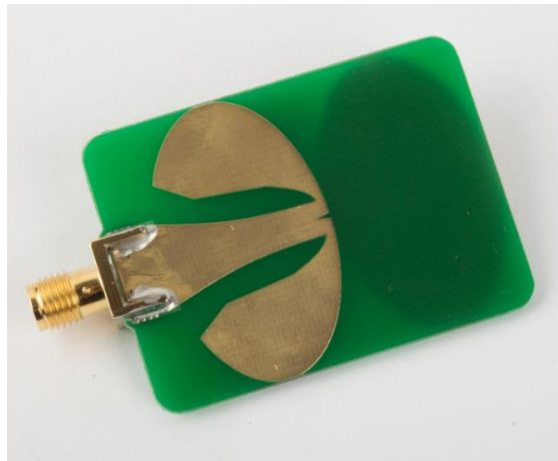


Figure 3.34 - Deepace Antenna Ground Plane

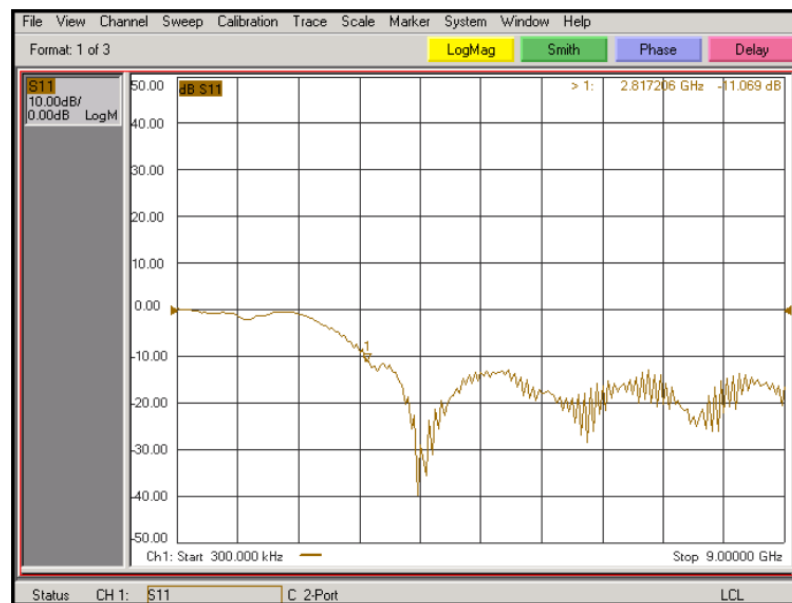


Figure 3.35 - Deepace Antenna S₁₁

3.4.2 XFDTD Simulation

The Deepace antenna was drawn on AutoCAD software and inserted into the XFDTD. AutoCAD software permits the implementation of the smallest details shown in the ground plane of the antenna to be used, as shown in Figure 3.36. In XFDTD software, the built design was including the two antennas facing each other, with a

separation distance of 10cm. The complete system was inserted in a 30x30x30cm box, and it is shown in Figure 3.37.

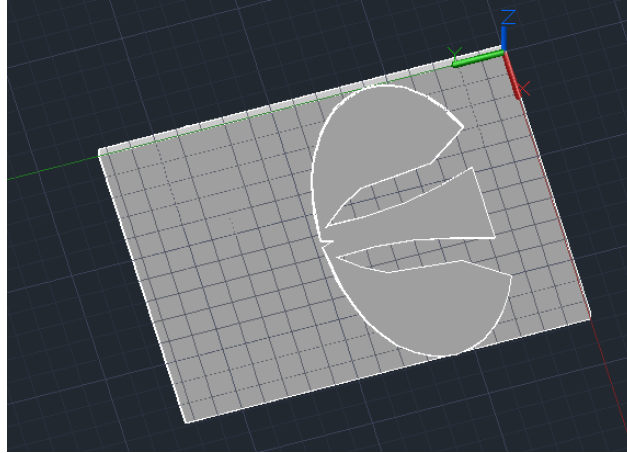


Figure 3.36 - AutoCAD Drawing of Deepace Antenna

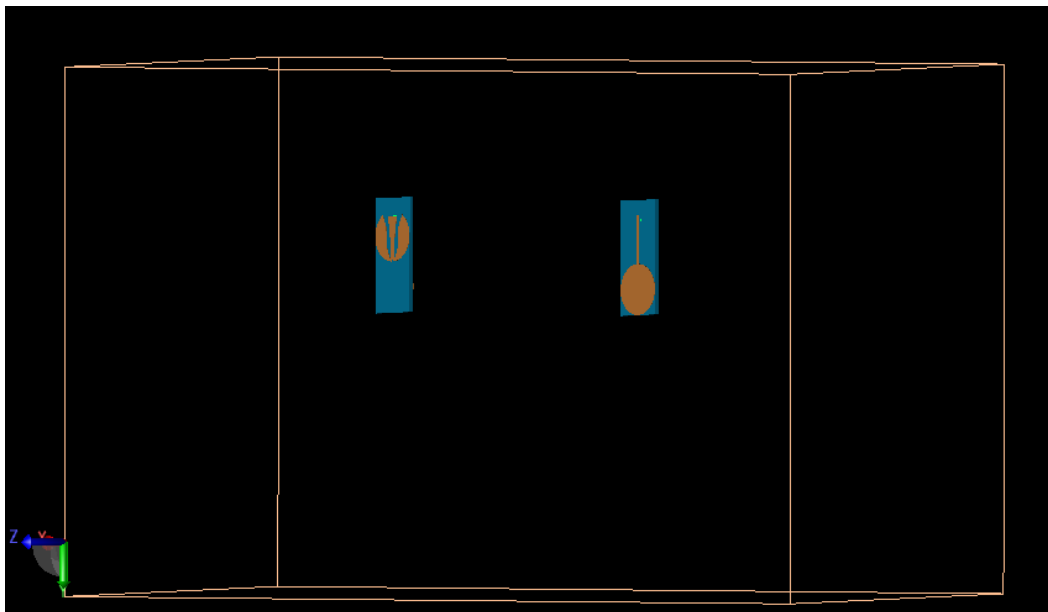


Figure 3.37 - Deeppace System

The grid base cell was generated automatically by the software, in a way to ensure smoothness at the curved edges of the Deeppace antenna used. The source is also a differentiated Gaussian pulse (DGP) in this case, located at the base of the Deeppace

antenna. The receiving Deeppace antenna was defined as a passive component where the received signal is computed.

After running the simulations in free space, some main parameters were extracted from the simulation results, such as the antenna impedance S_{11} shown in Figure 3.38, and the received signal S_{21} shown in Figure 3.39. Then, the material was changed to a soil type 1 (dielectric constant= 3 and conductivity=1mS/m) then soil type 2 (dielectric constant=4 and conductivity= 0 S/m), and soil type 3 (dielectric constant= 3 and conductivity = 0S/m). Figures 3.40, 3.41 and 3.42 show for the soil types 1, 2 and 3 respectively, the plot of S_{21} versus frequency.

In addition, the 2D radiation pattern of the Deeppace antenna was extracted at the constant plane of phi being 90° . This is called the E-plane pattern and it is shown in Figure 3.43. Similarly, the 2D radiation pattern of the antenna at constant phi of 0° is shown in Figure 3.44 and it is called the H-plane. Finally, the 3D pattern of the antenna is also shown in Figure 3.45.

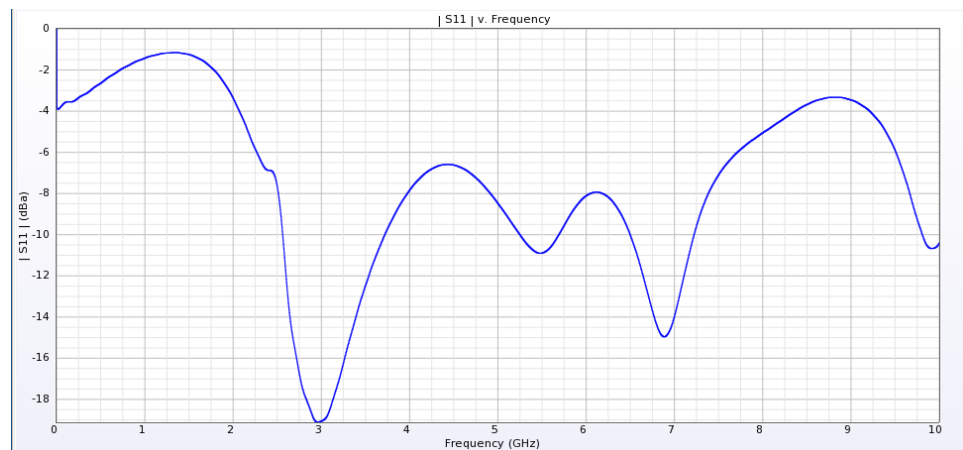
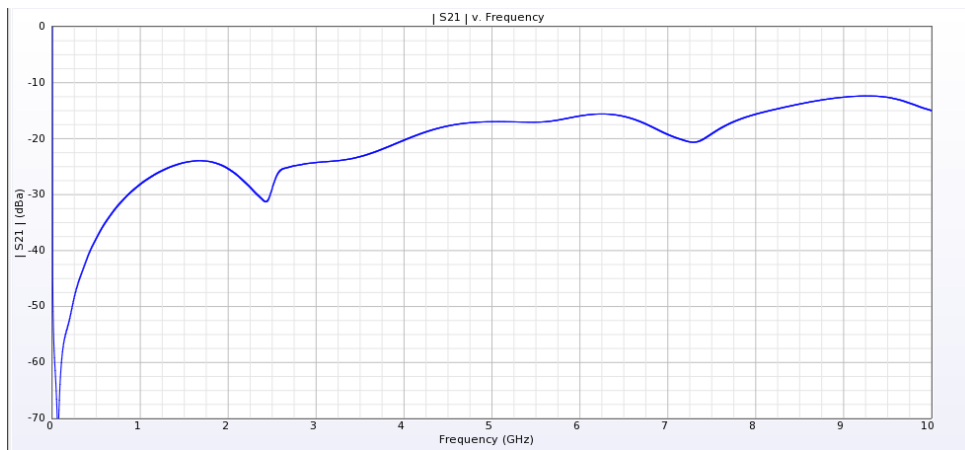
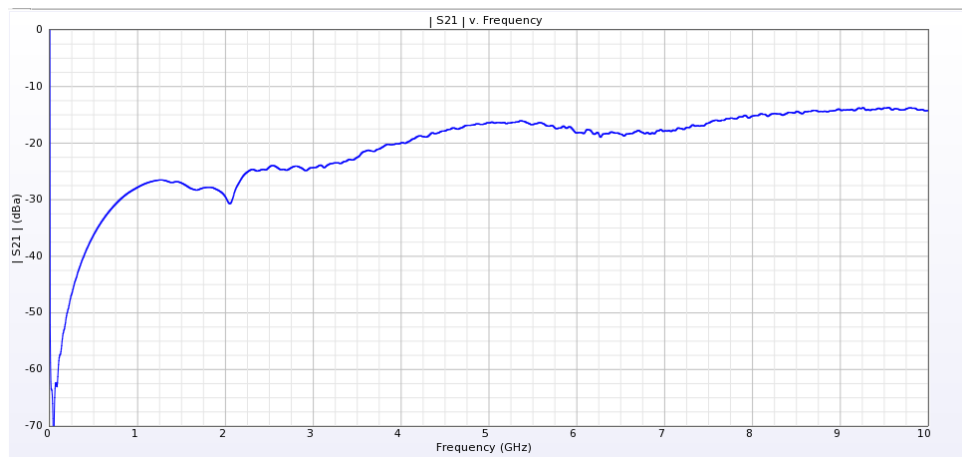
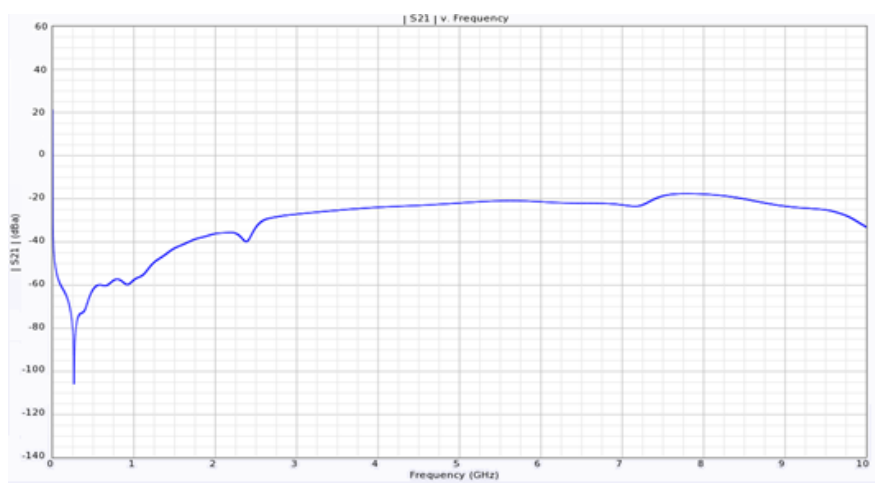


Figure 3.38 - S_{11} of Deeppace Antenna

Figure 3.39 - S_{21} Deep Space Free SpaceFigure 3.40 - S_{21} in Soil Type1Figure 3.41 - S_{21} in Soil Type2

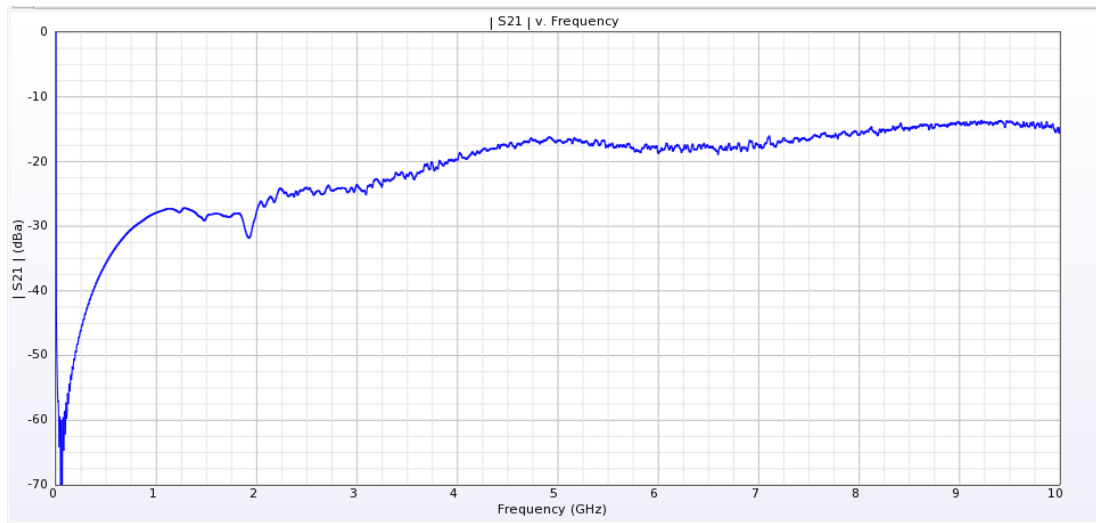
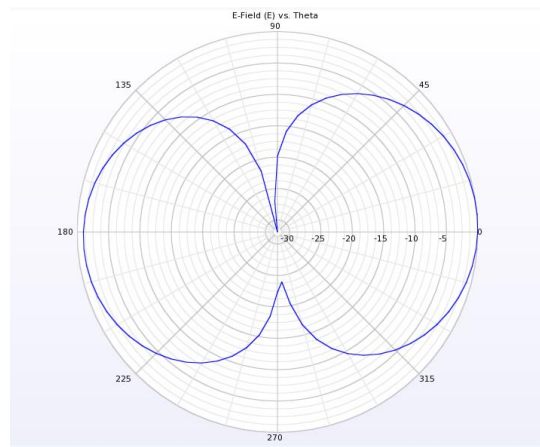
Figure 3.42 - S_{21} in Soil Type3

Figure 3.43 - Deepace E Plane

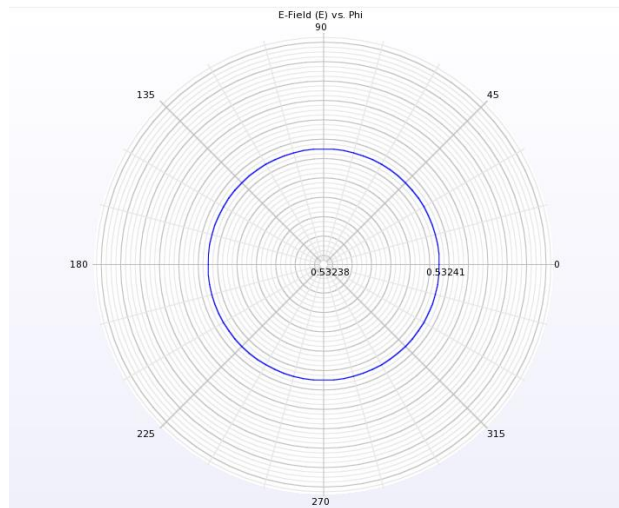


Figure 3.44 - Deeppace H Plane

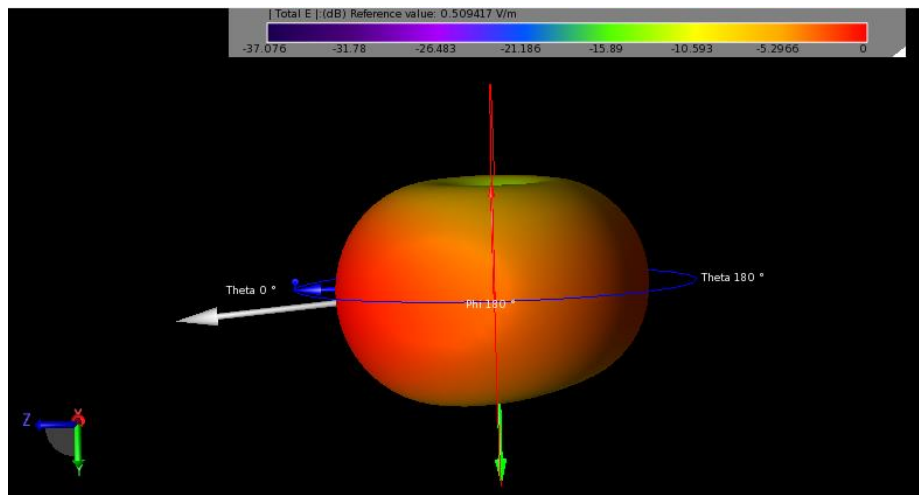


Figure 3.45 - Deeppace 3D Pattern

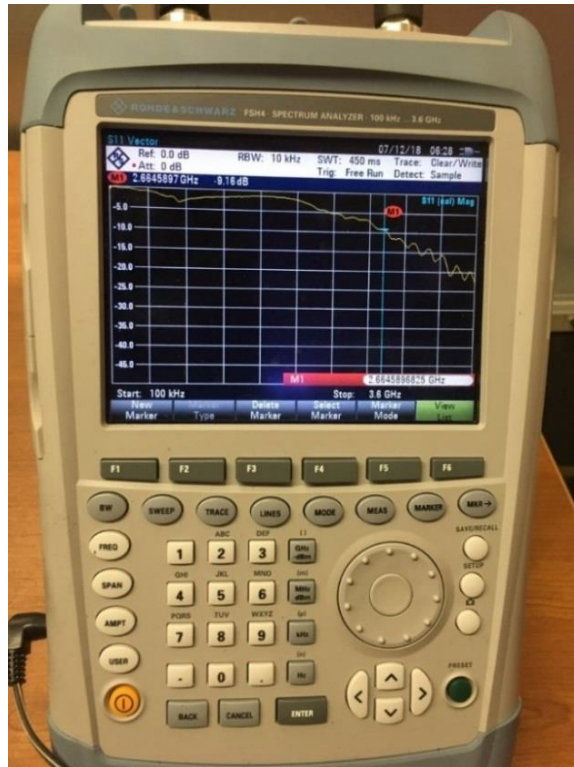
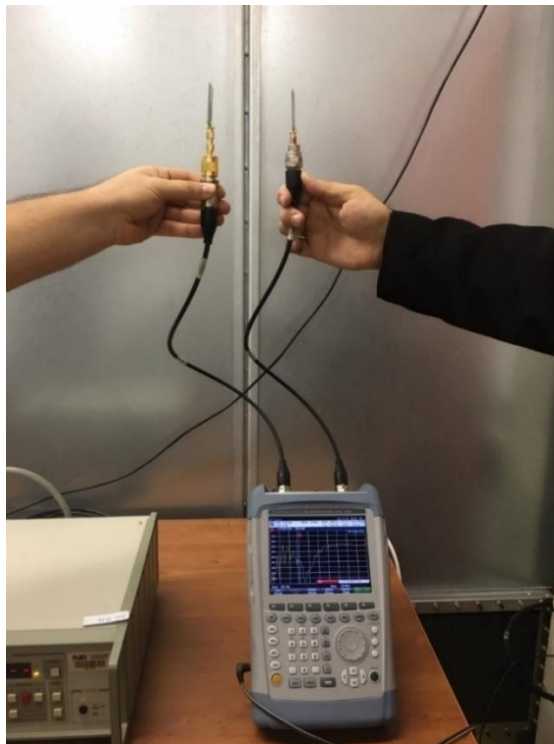
CHAPTER 4

Chapter 4 - MEASUREMENTS

4.1 Electrical Parameters Extracted

The Deepace antenna used was tested in the laboratory of Notre Dame University in order to check and compare its behavior and specifications with the theoretical data from its datasheet. To start with, the S_{11} of the antenna was tested using the available spectrum analyzer in the lab. To do so, the antenna was connected to the port of the analyzer through the SMA connector, as shown in Figure 4.1 below, and the value of S_{11} dropped below -10 dB at a frequency of 2.68 GHz indicating that the antenna is suitable for measurements from this frequency on.

Next, two Deepace antennas were placed facing each other, one playing the role of the transmitting antenna, and the other is the receiving one. The distance between them was approximated to be 10cm, matching the distance to be used in the probe. At this positioning shown in Figure 4.2, the S_{21} vector was measured. The result is shown in Figure 4.3.

Figure 4.1 - S_{11} Vector MeasuredFigure 4.2 - S_{21} Measuring Position

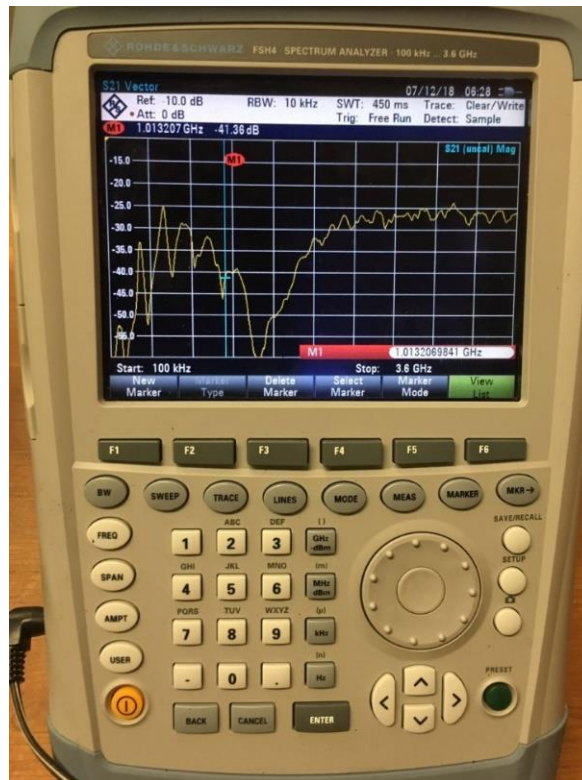


Figure 4.3 - S_{21} Vector Measured

As shown in Figure 4.3, S_{21} value was found out to be around -25dB at frequencies above 2.7 GHz. Even when rotation the antenna as shown in Figure 4.4, the S_{21} value remained acceptable indicating that the receiving antenna was still detecting a signal from the transmitter. However, in the position shown in Figure 4.5, the S_{21} value dropped to -45dB, verifying the 2D plot of the E Plane in the simulation section.

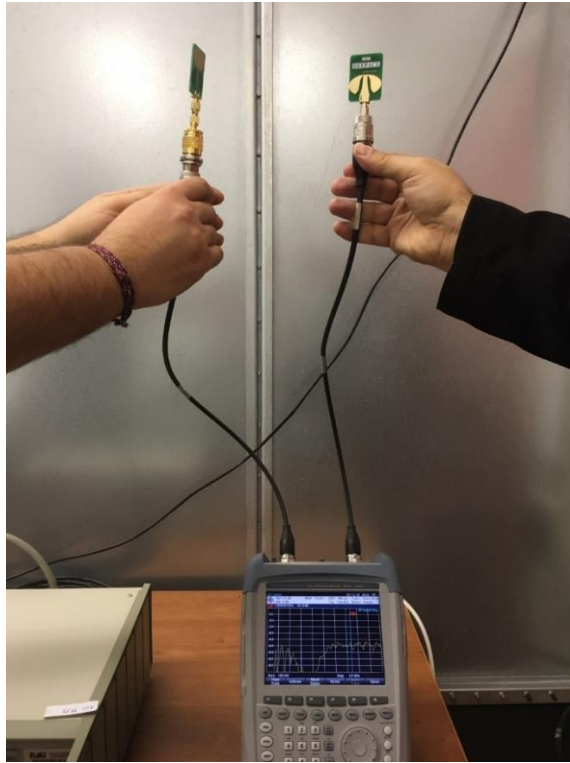


Figure 4.4 - S_{21} Positioning Rotated

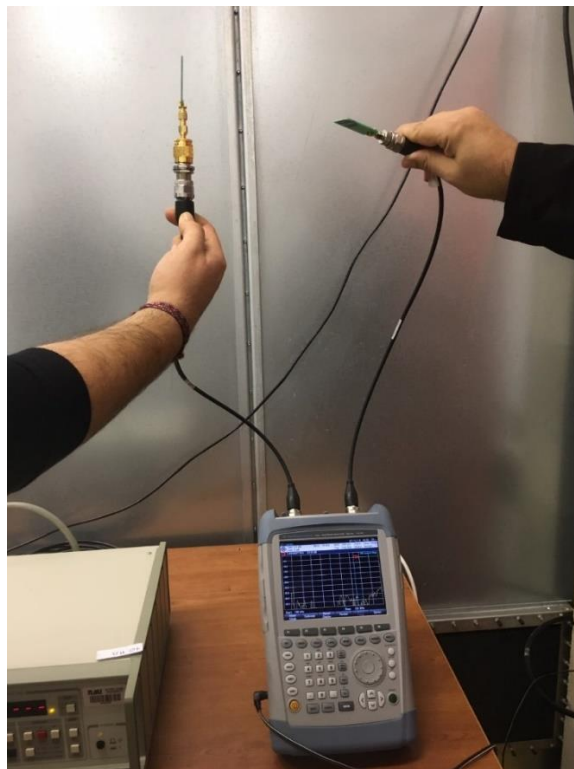


Figure 4.5 - S_{21} Second Positioning Rotated

Some additional measurements were executed in the anechoic chamber at NDU, for the purpose of extracting the E plane and H plane of the Deepace antenna. The first position of the Deepace antenna to be tested is shown in Figure 4.6. It is used to measure the E Plane pattern of the antenna. The results computed at 4 GHz by the software are shown in Figure 4.7, which prove that the measurements comply with the simulations results. In addition, Figure 4.8 shows the same plot at a frequency of 5 GHz.

Similarly, the measurements were repeated with the antenna position changed to the one shown in Figure 4.9. In this case, the antenna in the anechoic chamber shall be also rotated to the position shown in Figure 4.10. The H Plane was measured at 4 GHz and the results are shown in Figure 4.11. Next, the frequency was changed to 5 GHz, and then 2 GHz to observe the major changes. The results are shown in Figures 4.12 and 4.13 respectively.

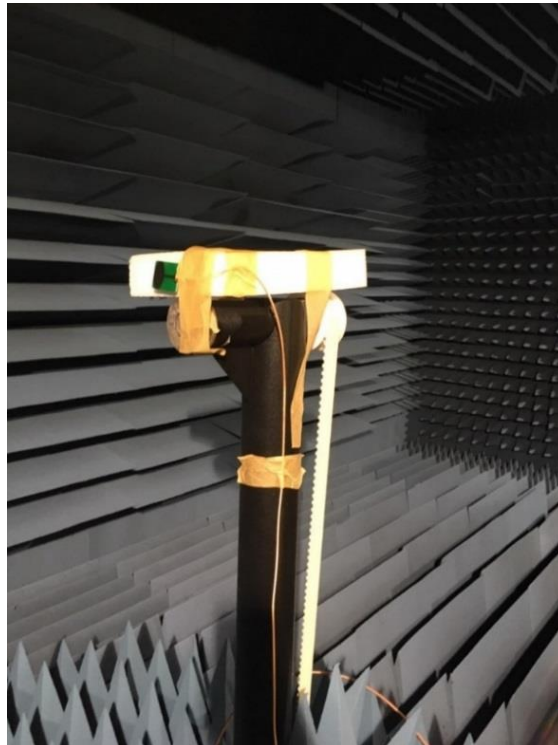


Figure 4.6 - E Plane Measurement Position

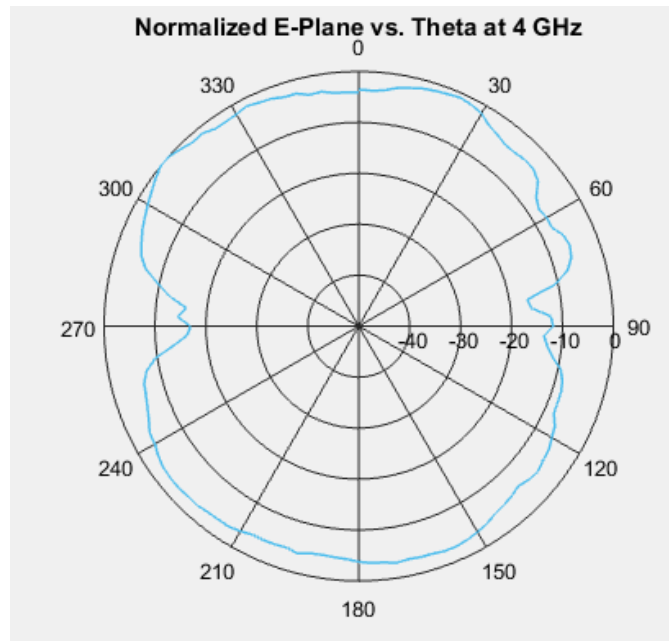


Figure 4.7 – Normalized E Plane Measured at 4 GHz

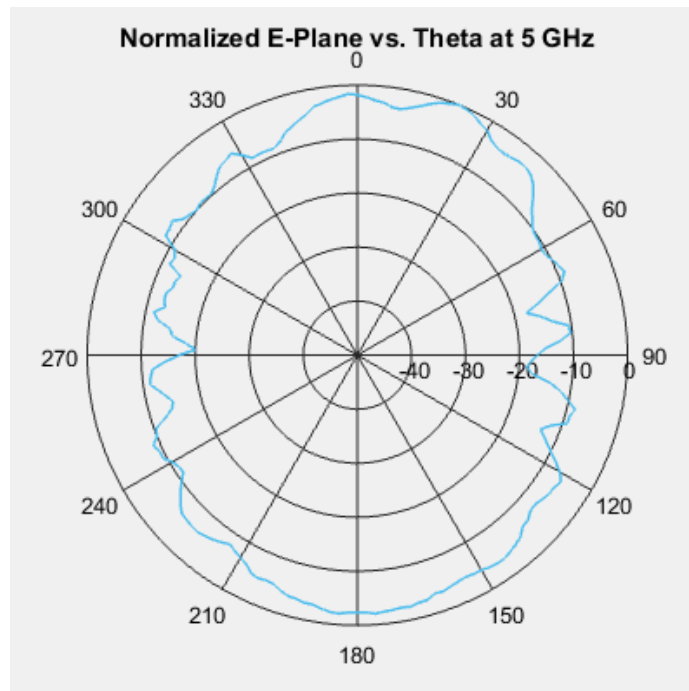


Figure 4.8 – Normalized E Plane Measured at 5 GHz

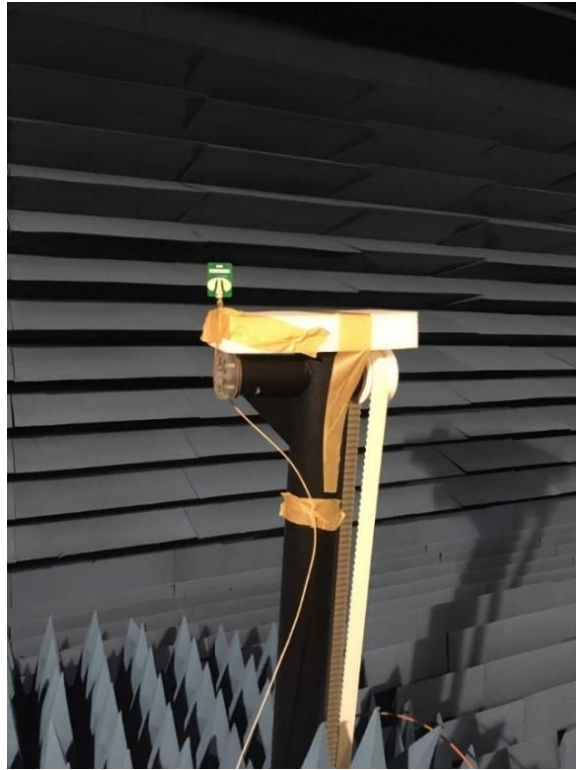


Figure 4.9 - H Plane Measurement Position

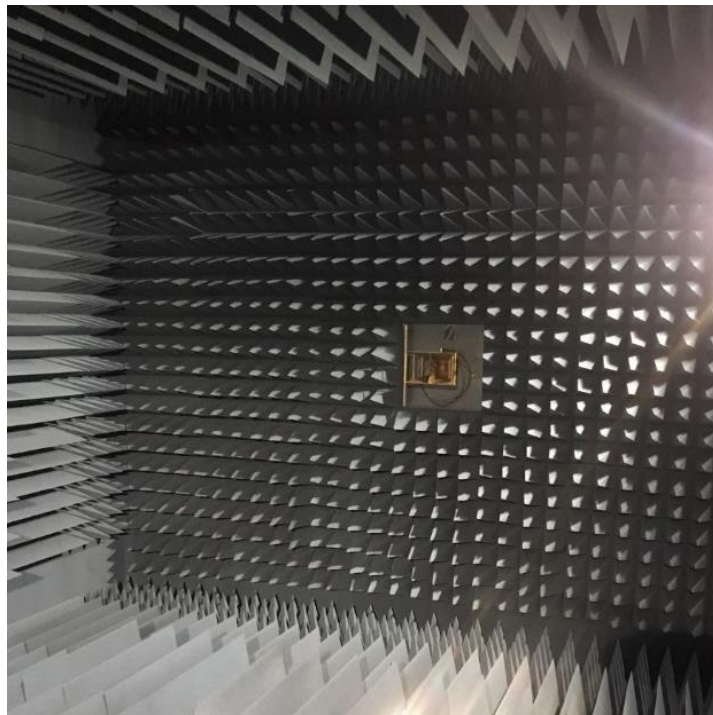


Figure 4.10 - Anechoic Chamber Antenna Position

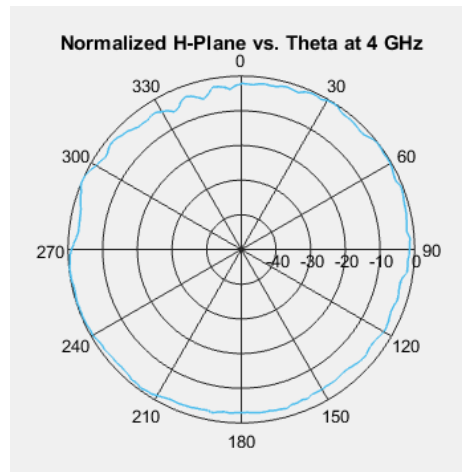


Figure 4.11 – Normalized H Plane Measured at 4 GHz

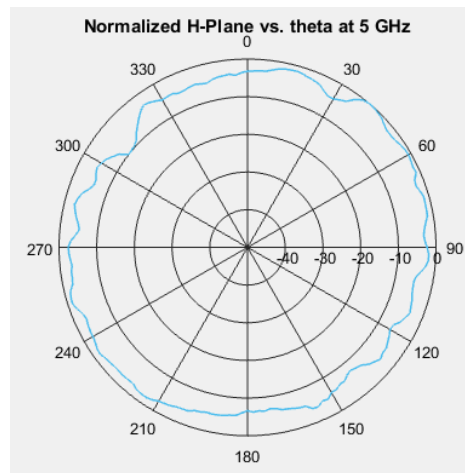


Figure 4.12 – Normalized H Plane Measured at 5 GHz

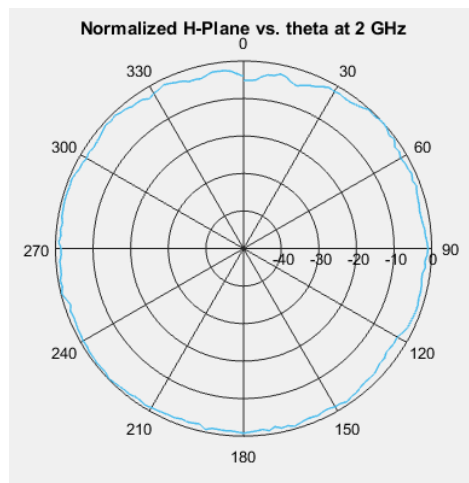


Figure 4.13 – Normalized H Plane Measured at 2 GHz

Next, the transmitting and receiving antennas were connected to a network analyzer, in order to visualize the needed results at the frequencies of operation of the Deepace antenna.

A network analyzer is a device that provides a frequency swept signal to a 2-port network and measures its S-parameters. For this purpose, the network analyzer shall be calibrated in order to minimize the effect of the cables, connectors and all the accessories needed for the connections. That way, the reference plane of measurements will be set to be the top of the cables used for the connections. The network analyzer used is the E5071C, ENA series from Agilent technologies. It is shown in Figure 4.14, together with the calibration unit used. Once calibrated, the values of S_{11} of the antenna were measured as shown in Figure 4.15, and the measurement of S_{21} in free space with a separation distance of 10cm between the two antennas is shown in Figure 4.16.

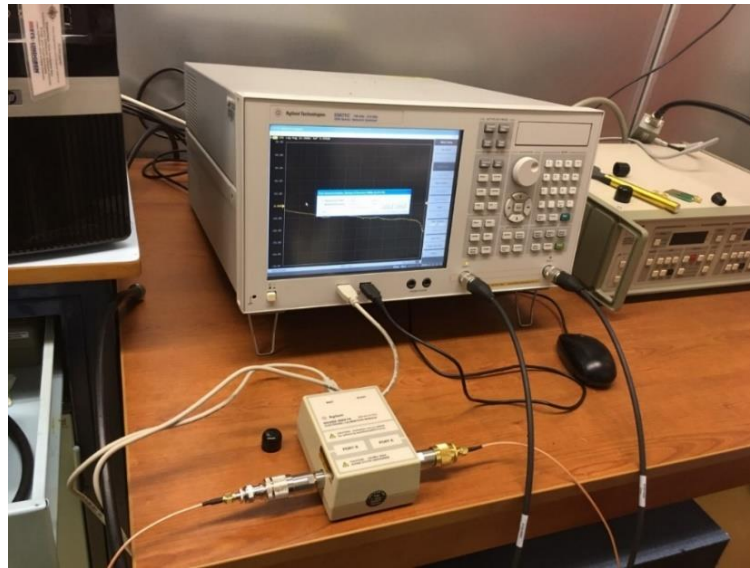


Figure 4.14 - Calibration of Network Analyzer

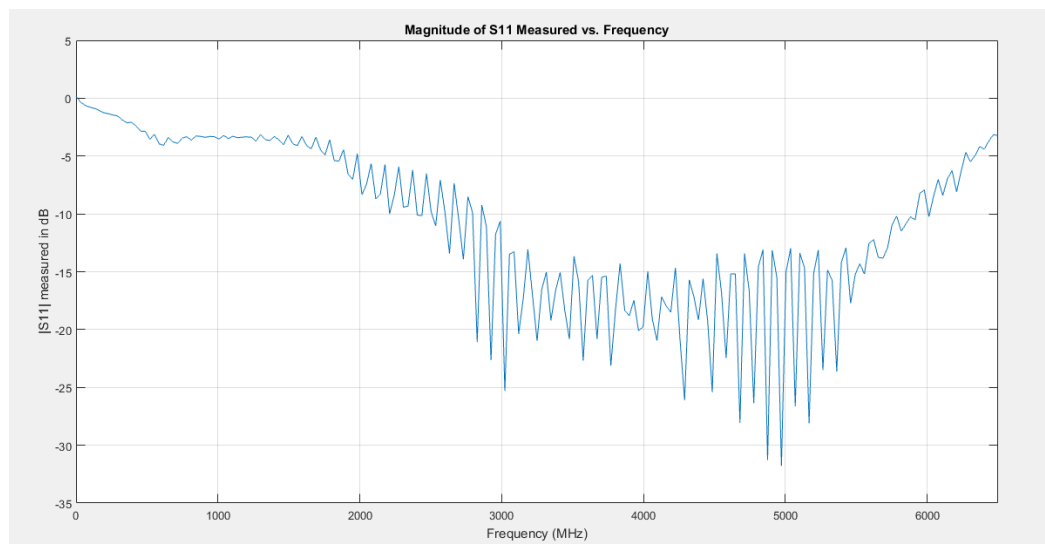


Figure 4.15 - S_{11} Measured by Network Analyzer

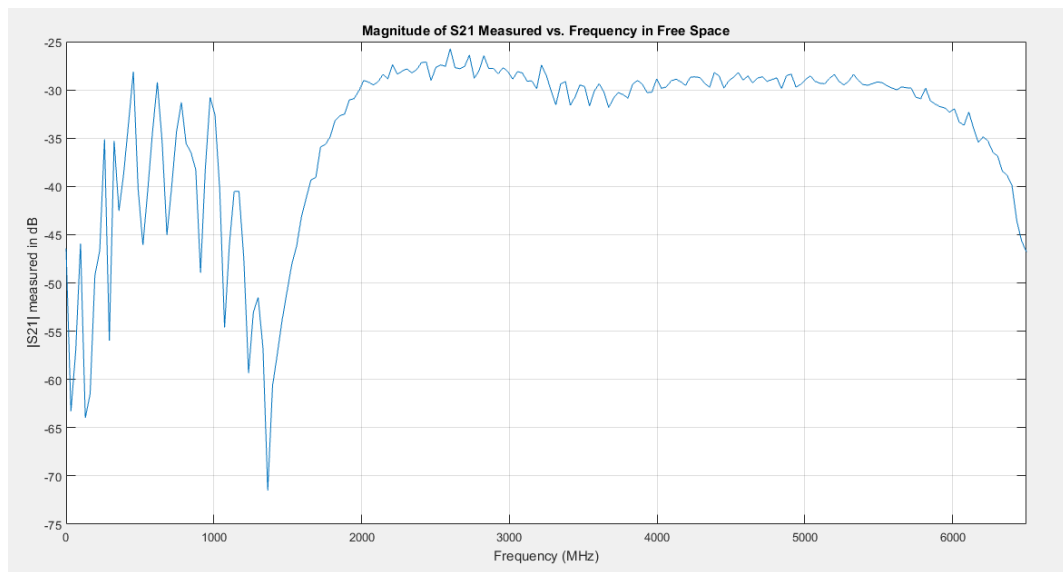


Figure 4.16 - S_{21} Measured by Network Analyzer

Some particular cases can be read from the cursors. For example, the S_{11} at a frequency of 2 GHz was measured to be -1.72 dB, whereas at 6 GHz it was found out to have a value of -14.22dB. Concerning the S_{21} plot, the cursors show that at 2 GHz, the value of S_{21} was measured by the network analyzer to be -32.23 dB, whereas at 6 GHz it was found out to be -31.13dB.

The phase plot was also extracted when the antennas were placed facing each other in free space. The disposition and the plot are shown in Figure 4.17 and 4.18 respectively. The same plot was extracted when an absorbing material was placed between the transmitting and receiving antennas as shown in Figure 4.19 and 4.20.

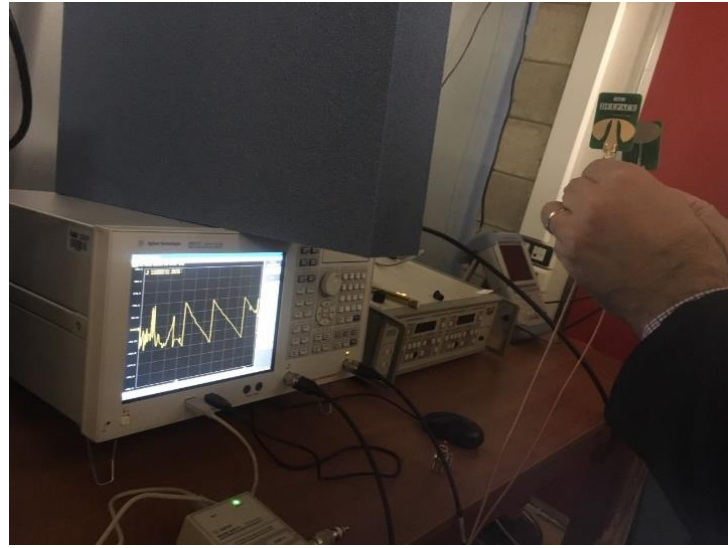
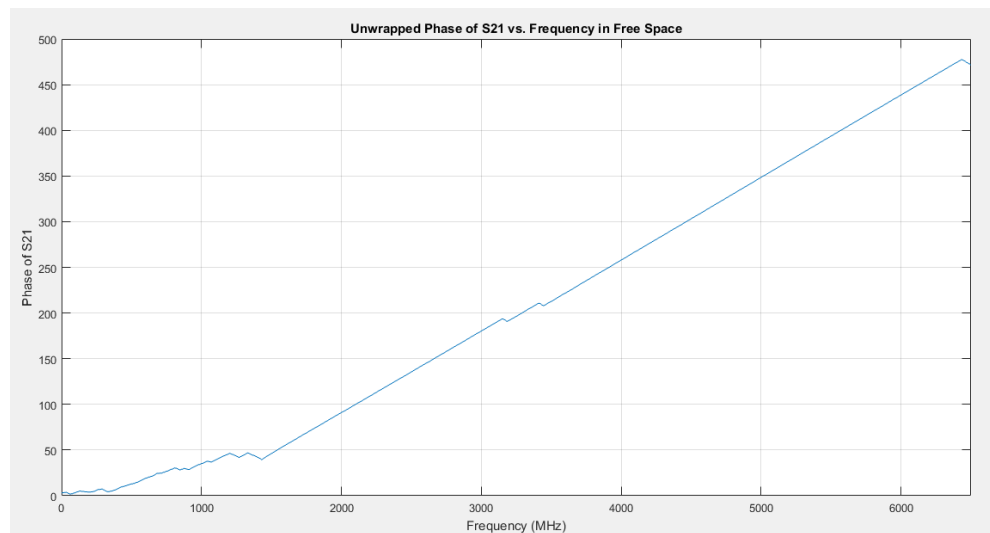


Figure 4.17 - Free Space Position

Figure 4.18 - Free Space Phase of S_{21}

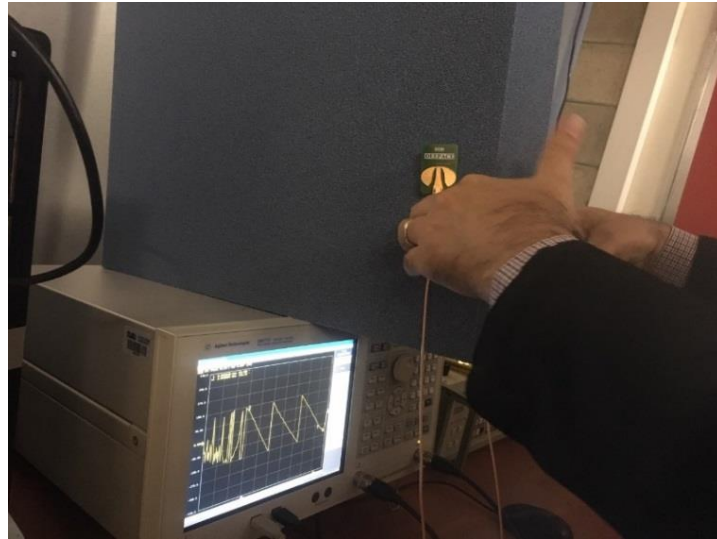


Figure 4.19 - Absorber Positioning

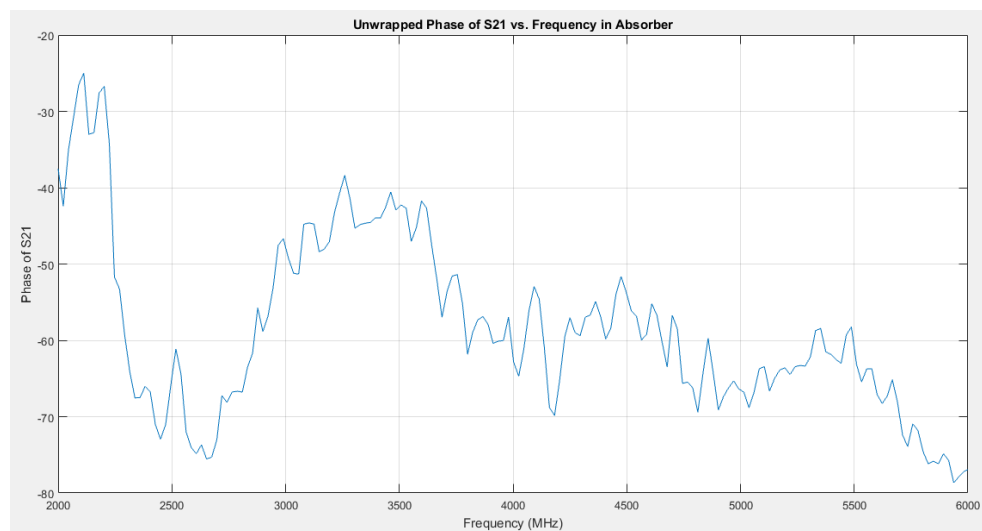


Figure 4.20 - Phase of S₂₁ in Absorber

The first stage of the system construction is shown in Figure 4.21.



Figure 4.21 - System Setting Out

To do so, a plastic box of 40x30x25cm was filled with the soil to be tested. The two antennas, the transmitting and the receiving one, were inserted into the soil at a depth of 10cm, and they were placed facing each other with a separating distance of 10cm. Before running the simulations and extracting the measurements, the system needed to be isolated from the surrounding in order to minimize all the undesired effects. In order to achieve this purpose, the absorbing material was used to create a perfectly matched layer surrounding the system, prohibiting the waves from reflecting at the edges of the system and being detected by either of the antennas, creating any unwanted disturbance to the measurements. The built system with the antennas embedded in the selected soil is shown in Figure 4.23.

The soil used for the measurements is called Ottawa sand. It is a naturally rounded grain sand made of almost purely quartz, hence most of its electrical properties follow the ones of quartz. Ottawa sand is mainly used for testing hydraulic cement. Its electrical permittivity is approximated to be between 4.5 and 5 at frequencies around 0.5 GHz. The simulation on the XFDTD software with the Ottawa sand used, shows the S_{21} of Figure 4.22.

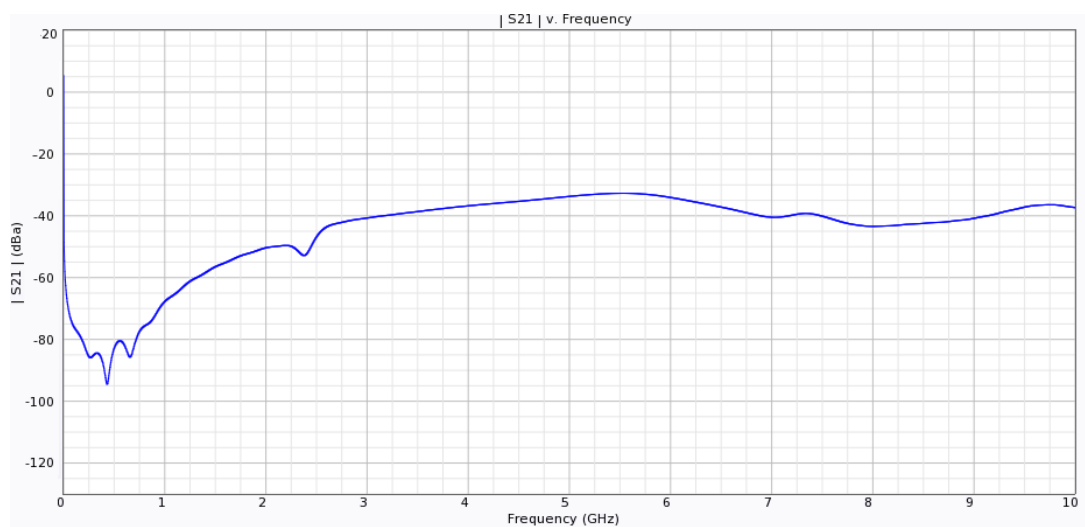


Figure 4.22 - S_{21} of Ottawa Sand

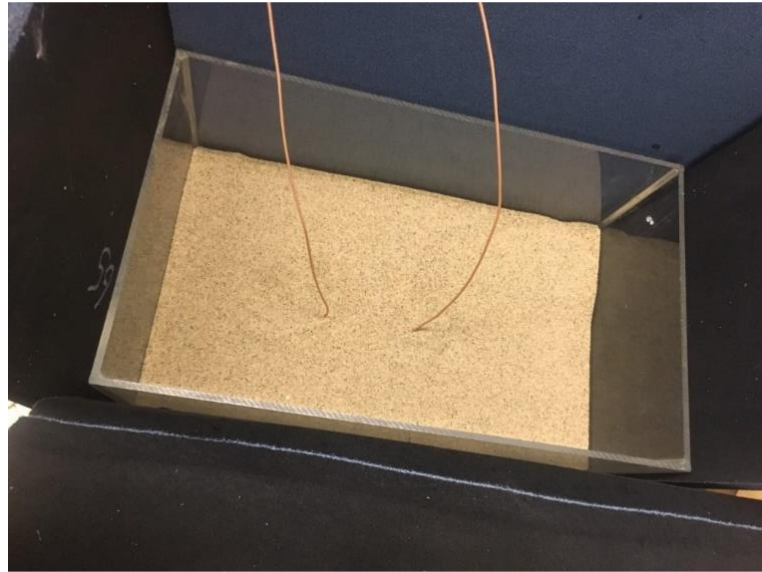


Figure 4.23 - Complete Probe with Antennas

In order to observe the changes in the gotten S_{21} versus the depth of the antennas in soil, multiple measurements were done. First, the antennas were placed facing each other at a depth of 5cm from the soil surface, and the data was collected accordingly. Similarly, the measurements were repeated by inserting the antennas deeper in the soil structure, and the data was collected at a depth of 10cm and 15cm.

For the comparison and observations to be clearer, the Matlab software was used in order to plot the S_{21} magnitude in the three cases of depths, and S_{21} phase in the same cases on the same graph. The results are shown in Figures 4.24 and 4.25 respectively. As shown, three curves are represented. The blue one corresponds to the results when the antennas were inserted 5cm into the Ottawa sand. The red plot corresponds to the results at antenna depth of 10cm from the soil surface. Finally, the orange curve is the

one to represent the results of the measurements when the antennas were placed deeper in the soil, at approximately 15cm depth from the soil surface level.

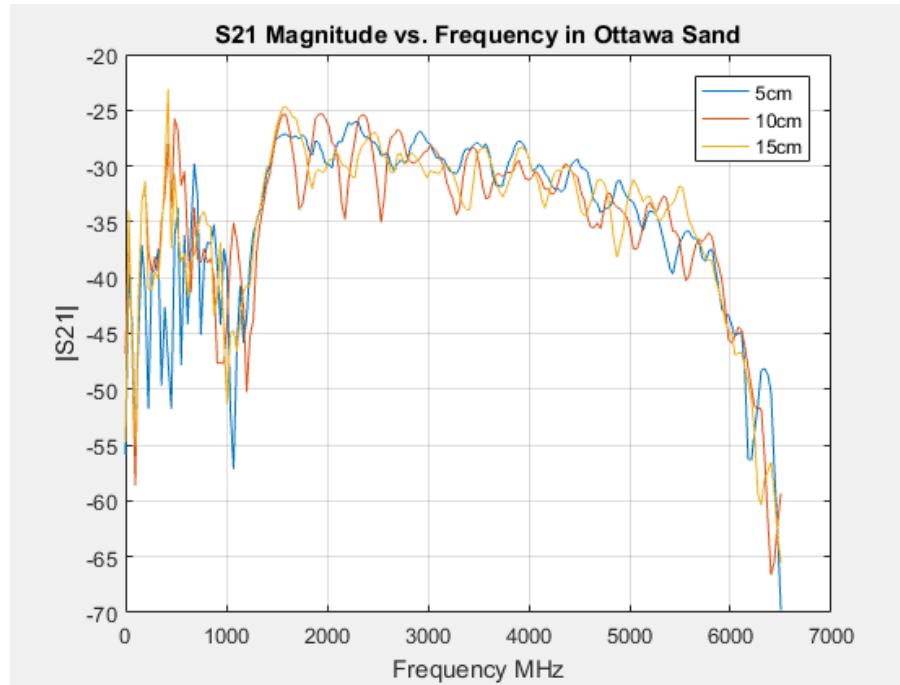


Figure 4.24 - $|S_{21}|$ vs. frequency in Ottawa Sand at Different Depths

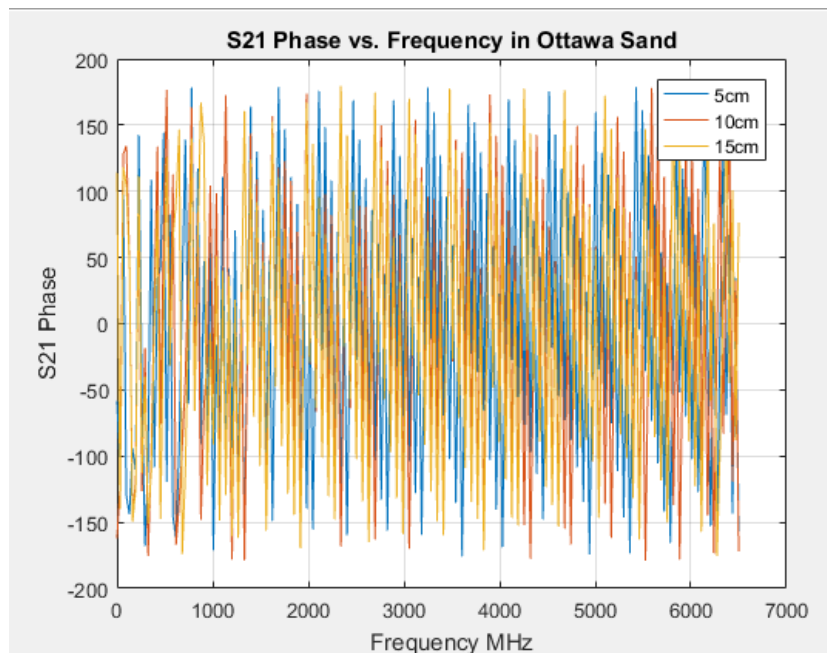


Figure 4.25 - S_{21} Phase vs. Frequency in Ottawa Sand at Different Depths

Next, the same measurements were performed on a beeswax sample, as shown in Figure 4.26. The absorbers were installed all around in order to minimize the reflections from the separation surface between beeswax and free space. The beeswax has a theoretical permittivity of around 2.8, which will be extracted in the observation part. Of course, the beeswax electrical properties may vary depending on the selected sample. In fact, the properties depend highly on the origin of honeybees, and any change in the acidity, temperature and other factors may affect the electrical permittivity and conductivity of the sample.

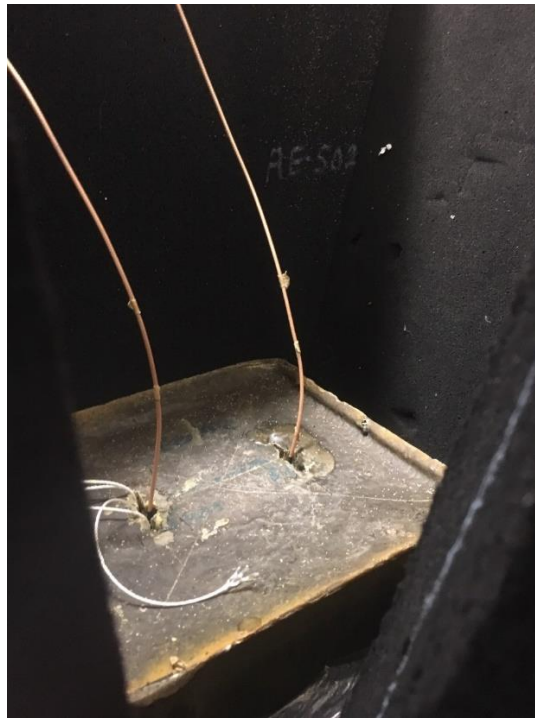


Figure 4.26 - Beeswax Measurement

Similarly, the S_{21} measurements were extracted in the lab for the case of a sandstone. The used stone was drilled to create two opposite holes separated by 10cm, in which the antennas were inserted. The used stone has a geometry of 25x25x20cm, and its details are shown in Figure 4.27. The sandstone usually has a relative

permittivity of 4. However, this property may also vary between one sample and another depending on its composition, moisture level, temperature, and other factors. The installation and measurement of S_{21} between the transmitting and receiving antennas in sandstone is shown in Figure 4.28.

In addition, the measurements were performed on a clay sample, shown in Figure 4.29. Finally, the measurements were also performed on an arbitrary soil sample near NDU.



Figure 4.27 - Sand Stone



Figure 4.28 – Sand Stone Measurements



Figure 4.29 – Clay Sample

4.2 Extraction of Parameters

The main purpose of this study was to be able to extract the soil parameters with in-situ measurements. To verify the success of the project, an observation and analysis was made based on the Ottawa sand simulation on XFDTD, and real measurements performed in the NDU Laboratory. To do so, a wider database was needed to be constructed, showing the variations of the magnitude of S_{21} with the change of soil permittivity at the desired frequency of interest, with the conductivity parameters fixed at $\sigma=0\text{S/m}$ and $\sigma=1\text{mS/m}$. From consecutive FDTD simulations for different soil types, the results at 3 GHz shown in the Table 4.1 below were extracted and used as a reference. It should be noted that the magnitude of S_{21} of table 4.1 was normalized with reference of the magnitude of S_{21} in free space simulated. The phase is unwrapped and referenced to the value at 2 GHz. Table 4.2 shows the results at 4 GHz, Table 4.3 shows the results at 5 GHz, and Table 4.4 shows the results at 6 GHz. Similarly, the measured values in the laboratory were also normalized reference to the free space measurements performed.

Table 4.1 - S_{21} Magnitude and Phase Normalized Database at 3 GHz

Soil Permittivity/ Soil Conductivity	$\sigma=0\text{S/m}$	$\sigma=40\text{mS/m}$	$\sigma=100\text{mS/m}$	$\sigma=300\text{mS/m}$	$\sigma=500\text{mS/m}$
$\epsilon_r=3$	4dB, -110°	2 dB, -100°	-2dB, -90°	-12dB, -50°	-18dB, -40°
$\epsilon_r=5$	-1dB, -340°	-5dB, -320°	-10dB, -180°	-8dB, -100°	-13dB, -100°
$\epsilon_r=7$	8dB, -250°	7dB, -200°	5dB, -250°	-3dB, -100°	-9dB, -120°

Table 4.2 - S_{21} Magnitude and Phase Normalized Database at 4 GHz

Soil Permittivity/ Soil Conductivity	$\sigma=0\text{S/m}$	$\sigma=1\text{mS/m}$	$\sigma=10\text{mS/m}$	$\sigma=20\text{mS/m}$	$\sigma=30\text{mS/m}$
$\epsilon_r=3$	-2.5dB, -90°	-3dB, -110°	-4dB, -120°	-12dB, -100°	-20 dB, -100°
$\epsilon_r=5$	8dB, -590°	6dB, -540°	3dB, -280°	-6dB, -200°	-14 dB, -220°
$\epsilon_r=7$	9dB, -600°	8dB, -500°	5 dB, -550°	-3dB, -350°	-11 dB, -350°

Table 4.3 - S_{21} Magnitude and Phase Normalized Database at 5 GHz

Soil Permittivity/ Soil Conductivity	$\sigma=0\text{S/m}$	$\sigma=1\text{mS/m}$	$\sigma=10\text{mS/m}$	$\sigma=20\text{mS/m}$	$\sigma=30\text{mS/m}$
$\epsilon_r=3$	3.5 dB, -220°	1.5dB, -220°	-3dB, -220°	-13 dB, -180	-23dB, -160°
$\epsilon_r=5$	6 dB, -840°	4 dB, -790°	0 dB, -530°	-13dB, -450°	-22dB, -350°
$\epsilon_r=7$	8 dB, -1000°	7 dB, -900°	4 dB, -950°	-6 dB, -800°	-14dB, -550°

Table 4.4 - S_{21} Magnitude and Phase Normalized Database at 6 GHz

Soil Permittivity/ Soil Conductivity	$\sigma=0\text{S/m}$	$\sigma=1\text{mS/m}$	$\sigma=10\text{mS/m}$	$\sigma=20\text{mS/m}$	$\sigma=30\text{mS/m}$
$\epsilon_r=3$	2 dB, -380°	-1dB, -380°	-4.5dB, -360°	-17.5dB, -280°	-28dB, -210°
$\epsilon_r=5$	7dB, -1140°	4dB, -1120°	1 dB, -880°	-11 dB, -800°	-23dB, -400°
$\epsilon_r=7$	9dB, -1380°	7.5dB, -1300°	4 dB, -1350°	-5 dB, -1150°	-15dB, -800°

The stated values were extracted from the magnitude of S_{21} in each material type normalized with reference of the magnitude of S_{21} in free space. Whenever the measurements are done in-situ, the measured value of the magnitude of S_{21} will be transmitted to a specified software that will compare the measured value with the matrix

pre-saved in the database. The closest point of intersection to the measured value will correspond to the ϵ_r , and σ values accordingly. In the case of Ottawa sand, the measured values obtained are shown in Table 4.5 below, and the corresponding values of the permittivity and conductivity are also shown based on the comparison with the simulated results.

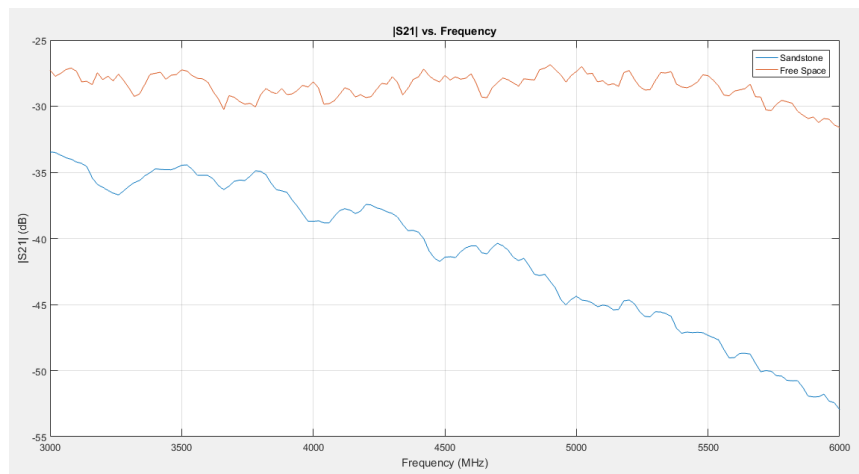
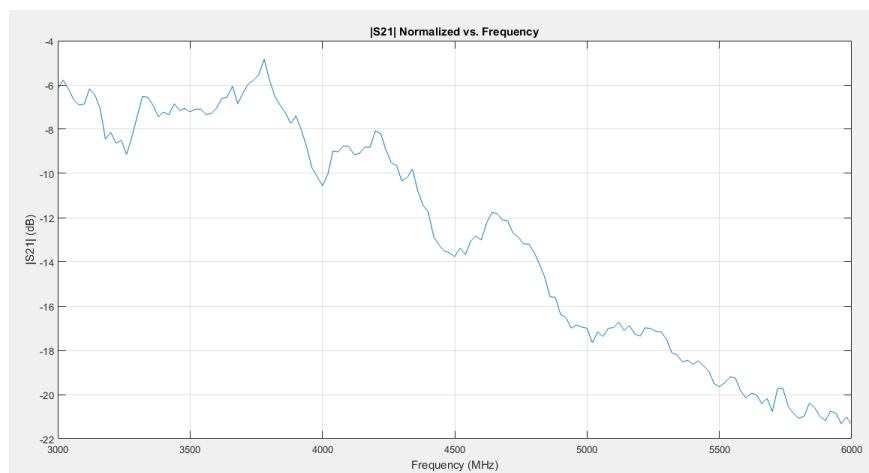
Table 4.5 – Ottawa Sand Measurements

Ottawa Sand			
Frequency (GHz)	Normalized Measured S21 Mag(dB),Phase(deg)	ϵ_r,	σ(mS/m)
3	0, -100	3	80
4	0, -160	3.5	40*
5	-2, -300	3	80
6	-8, -450	3	200

The next example implemented in the lab was to examine the parameters of the sand stone. For this purpose, a sample was brought. From the measurements at 3, 4, 5 and 6 GHz, Table 4.6 could be extracted as shown. The plot of the measured magnitude of S_{21} in free space and in the sandstone sample is shown in Figure 4.30. Hence, the normalized magnitude of S_{21} in sandstone with respect to free space was plot in Figure 4.31, and the normalized phase of S_{21} in sandstone with respect to free space is shown in Figure 4.32.

Table 4.6 – Sandstone Measurements

Sandstone			
Frequency (GHz)	Normalized Measured S21 Mag(dB),Phase(deg)	ϵ_r	σ (mS/m)
3	-6, -200	5	80
4	-10, -400	7	500
5	-17, -570	7.5	500
6	-21, -720	7	600*

Figure 4.30 - S_{21} vs. Frequency in Free Space and SandstoneFigure 4.31 - Normalized Magnitude of S_{21} in Sand Stone

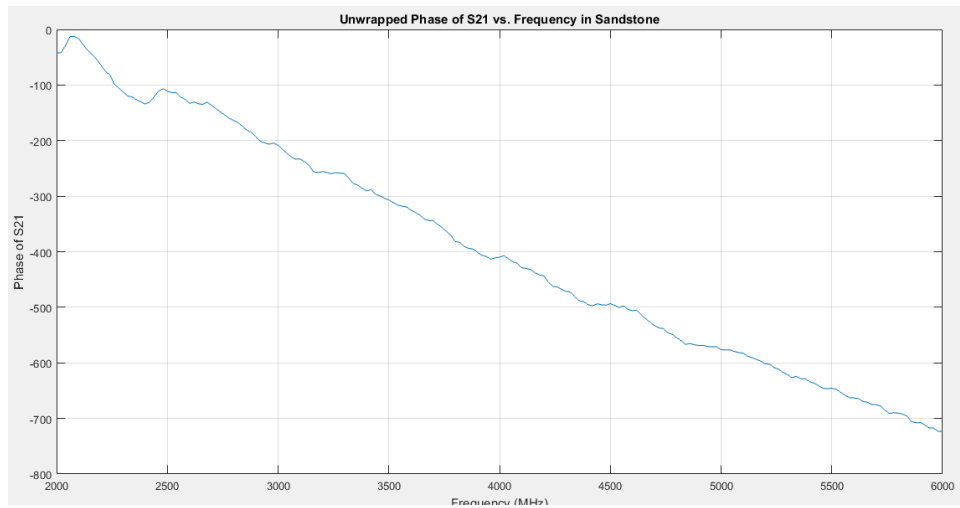


Figure 4.32 - Normalized Phase of S_{21} in Sandstone

Next, for the tested sample of clay, the S_{21} magnitude obtained is shown in Figures 4.33. By comparing the values, Table 4.7 could be extracted.

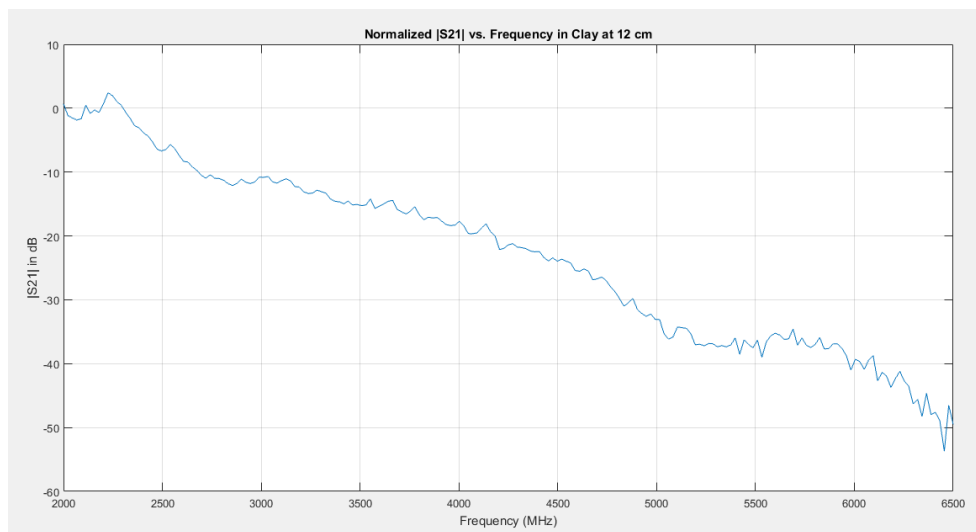


Figure 4.33 – Magnitude of S_{21} vs. Frequency in Clay

Table 4.7 – Clay Measurements

Clay (NDU Sample)			
Frequency (GHz)	Normalized S21 Mag(dB),Phase(deg)	Measured ϵ_r,	σ(mS/m)
3	-11,-100	5	400
4	-19,-200	5	700*
5	-35, -330	5	800*
6	-40, -400	5	1000*

For the soil sample selected near NDU, the S_{21} magnitude obtained is shown in Figure 4.34. By comparing the values, Table 4.8 could be extracted.

Table 4.8 – Soil Sample Measurements

Soil (NDU Sample)			
Frequency (GHz)	Normalized S21 Mag(dB),Phase(deg)	Measured ϵ_r,	σ(mS/m)
3	-6, -100	7	400
4	-10, -220	5	400
5	-17, -350	5	400
6	-30, -500	5	700*

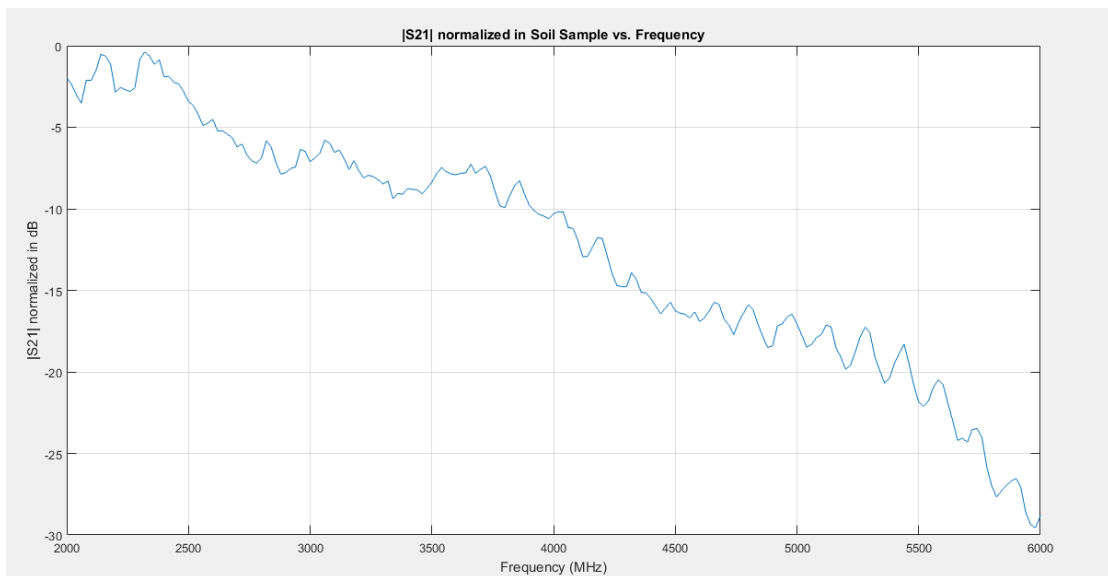


Figure 4.34 - Magnitude of S_{21} vs. Frequency in Random Soil

Obviously, the accuracy of the extracted results can be enhanced by having a wider pre-saved database and including more variety in the values of the permittivity and conductivity.

CHAPTER 5

Chapter 5 - SUMMARY, CONCLUSION AND FUTURE WORK

In this Chapter, a detailed summary of this report is outlined, along with a brief conclusion, followed by suggestions on ways to improve the report and expand it with additional information.

5.1 Summary

In summary, this report presented the design of a new wideband probe for the in-situ measurements of soil characteristics. The probe can be used with devices such as GPR and radiometers to help enhance their detecting capabilities. Three-dimensional FDTD simulations were performed with soil types of different permittivity and conductivity values. It was observed that the received signal's amplitude and phase provide enough discrimination between different soil types. A prototype of the probe is constructed and some enhancements are still in progress. The simulation results will be used in conjunction with measurements to predict the electrical parameters of different materials.

5.2 Conclusion

In conclusion, after completing the study, it is necessary to note that the existence of a wider database affects directly the accuracy of the probe. In fact, an automated system shall be provided or developed to be used to match the measured value with the simulated ones in the fastest way, rather than referring to manual selection by the user.

Cost wise, the project was found to be feasible and affordable, specially that its type of cost is a one-time payment that will be invested at the beginning of the product execution. The software used to study, analyze and compare the data in order to get accurate results about the soil characteristics should also be taken into consideration. Another main component in the cost analysis is the running cost of the machine used, the charges of the engineers and the personals executing the work on site, known as the resources cost.

When moving to the cost-benefit analysis, the perception is different because the rewards of the projects in question are of very high value, as this project is designed to be used for humans' protection and to avoid risks. Therefore, this project has a very good cost to benefit ratio and is considered to be successful.

5.3 Future Work

After the studies performed, a wider database shall be created for the S₂₁ magnitude and phase for different soil types. The described device can be used in order to extract the main characteristics of the land needed by comparing the measurements to the database. This procedure can be done either in situ, which is preferable, or by performing the studies on a sample of the land.

For future observations, the simulated device may help in major enhancements for the landmine detections project. When the soil structure of the land is known, it is much easier to analyze its content and define its response. The received signal will be clearer when the effect of the soil itself is eliminated.

In short, the described device can be integrated in an already existing system used to scan and find the buried objects underground in the endangered lands when there is

a risk of landmines. This integration is helpful because it will reduce false alarm rates and enhance the performance of landmine detection devices. Hence, the clearance methods of landmines will be more helpful and all creatures mainly humans will be protected.

Another application of this work can be in the area of the internet of underground things (IOUT). When communications systems are used underground or in the soil we need to know the ground parameters in order to properly predict antenna pattern and impedance behavior [16]. The moisture level in the soil varies from one moment to the other, that's why the measurements of the soil parameters should be accurate and updated.

APPENDIX A

Landmine Detection Techniques

The methods used for landmines clearance started to be manual, and their progress is too slow compared to the high level of danger, requiring speed and effectiveness in the clearance methods used. Also, the majority of the mines are located in lands away from roads or unreachable by cars in case of emergencies. Some of the mine detection concepts search either for the metal characteristics in the mine, or in case the mine's body is plastic, the method will search for detecting bulk explosives based on chemical properties or physical properties of the mine. A Ground Penetrating Radar (GPR), is one of the methods currently used for landmines clearance. Other methods include metal detectors and thermal imaging.

The Electrical Impedance Tomography, EIT, is another method used for mine clearance. It uses electrical currents to detect the conductivity distribution of the area being scanned for mines. However, it requires physical contact with the ground which might detonate a mine. EIT is sensitive to electrical noise and its good performance is restricted for shallowly buried objects.

The X-Ray backscatter method passes photons through the object to create an image. It operates using focused beams and detectors to create the image, and it uses spatial filter to deconvolve the system's response. The product of the X-Ray backscatter is a high-quality image because of the small wavelength of the X-rays. It is also easy to implement since it already exists in medical industry. In addition, it is light in weight,

small size, portable, and it requires low energy because of the available isotopic sources. However, this device has a large size, and consequently it weighs a lot so it cannot be portable. Another limitation of this method is that it requires power to operate, so it cannot be carried to the land in order to do in-situ measurements. This method is also not functional for deep buried objects in the land, because it provides poor soil penetration reaching a depth of less than 10cm. It also requires a very long time to obtain the response image and process it. This device cannot be used in heterogeneous soil, since it is very sensitive to the smoothness of the ground, so the emitted radiations will face resistance and prevent the received signal to be detected properly.

On another hand, the infrared or hyper spectral method was also used for the mines' clearance procedure. This method detects the variations in the temperatures next to the mines, since they will be warmer. This method can be considered a non-thermal method, since it detects the light reflected by the areas nearby the landmines. The strength of this method is that it does not need any physical contact with the contaminated land, since it operates at a distance, and it scans large areas very quickly. It is also light in weight to be carried to the land. However, the infrared or hyper spectral method has a non-stable performance, as it can varies depending on the environmental changes. Another major limitation for this method id that its algorithm and model are not yet existing in order to operate. It should be noted that it is not suitable for close-in buried mines.

The acoustic or seismic clearance method works by pushing the object

underground to vibrate by sound or seismic waves, and it analyses the reflected sounds. This method senses differences in the mechanical properties of the objects found in the ground, which make it able to differentiate and identify them. This way, low false alarm rates will be faced. This method may be used to complement an existing method, taking into consideration that it is not affected by moisture and weather. Unfortunately, the weaknesses of this method include that it is not effective on frozen grounds, and it does not go very deep inside the soil because of the high attenuation faced. The performance of the acoustic method is limited by the slow speed of the vibration sensors, and the Doppler problems by the existing heavy vegetation.

The biological method used for mine clearance has a different way of operation. It detects the explosive vapor that is created by the mines. This method involves the usage of some animals trained to fulfill this job. For example, dogs and rats might succeed in this method due to their great sense of smell. Bees can also be used for detection purposes, by placing the target chemical in the bees' natural foraging area, making them search for it as food. Bacteria, a type that fluoresce in TNT is sprayed on the area and detection of fluorescent signals will come next. What might be good about this method, is that it detects explosive vapors at concentrations lower than those detected by chemical sensors, and it works under any environmental circumstances. The selection of the animals participating in the mines' clearance is very important; rats are low in weight and do not deploy mines while scanning the contaminated lands. The biological method can search and scan large areas in short time, especially when using TNT. Some of the weaknesses of this method, are that it has a variable performance depending on each dog, his behavior and his skills. It also needs training sessions to

prepare the testing animals properly. What is more dangerous, is that every while, weather conditions may cause explosive vapors to migrate away from the mine, leading to false detection or even the absence of detection while the mine still exists. If one follows the bees for clearance, the bees work under conditional weathers only, they do not work at temperatures below 40°F, which causes inability to track the bees' movements. Environmental limitations will play a role by introducing bacteria in the air, which is not welcomed, and make this method not function in dry soils. For the fluorescent detectors used, they are not very accurate.

The chemical method measures changes in fluorescence and electrical resistance. It measures the shift in the resonance frequency, or compares the spectral resonance with that of a reference material. It is small, lightweight, portable and easy to use. In addition, its prototype already exists which makes it ready to be used. This method cannot replace conventional methods unless a 100% of accuracy is reached, and it is not the case till the date. This method is also not reliable for metal cases, as it also has limitations in its performance in dry environments.

The bulk explosives, nuclear quadruple resonance method detects the specific chemical compounds needed. The chemical bonds in the explosives are tested and seen to resonate and induce electric potential. This detection strategy is specific to landmines, and has a high probability of detection, and it works in different soil conditions. However, the TNT provides weaker signals than other explosives making it harder to be detected. The radio frequencies used for this type of operation are also subject to interference causing false scanning and making the testing not possible for

metal cases as radio frequencies do not penetrate in metals. This type of detection cannot be made while in motion because of the SNR degradation, creating an additional disadvantage when using this clearance method.

The neutron distinguishes the intensity, energy, and other characteristics of the radiations emitted from atomic nuclei in explosives. Hence, the neutron method uses low strength source radiation making it need moderate costs, but its work is limited in moisture and it is sensitive to ground fluctuations.

The last stated method is the prodders and probes. This is a manual technique used to detect the nature of the object by delivering acoustic pulse, and getting feedback about the amount of force applied by the probe. This method is known to be effective, but it is not safe as it requires physical contact with the ground which might detonate a mine.

Consequently, it is not advised to use this method in grounds with lots of root structures.

This was a summary of the different approaches previously implemented and used to clear the existing landmines. In addition, it highlights the major strengths of each method, and it shows the limitations preventing it from going further and achieving a 100% full success and accuracy at a zero false alarm rate.

Different types of probes were used in the past to measure the dielectric constant of soil. Some of these methods only measure the real part of the permittivity, other methods are limited in their capability to measure properties at varying depths in the soil, some are not suited for in-situ measurements and still others measure soil

parameters at frequencies below 1 GHz.

APPENDIX B

Soil Types

GPR functions by emitting radio waves into the surface being scanned for mines, and detecting the reflected signals. Processing of the signals returned from the ground leads to the detection and identification of the buried targets. For proper processing of the signals one needs knowledge of the electrical parameters of the soil where the radar signal is traveling. Consequently, the GPR performance is highly dependent on the soil characteristics. GPR senses changes in dielectrics, so it can find wide variety of mines. It is light in weight, easy to operate, it detects all anomalies, metals and non-metals sensitive to complex iterations among mine metal content. It is sensitive to soil moistures and sensitive to the smoothness of the ground surface. GPR has a variable performance and a tradeoff frequency should be selected to manage between image quality and depth and accuracy needed.

A GPR has many applications in which it can be helpful. However, when it comes to applications of mine clearance, shallow depths and significantly high image qualities are desirable, so a GPR employs higher frequencies than those required for conventional applications. In this case, a GPR will become more sensitive to the heterogeneity of the soil surrounding the buried object, which results in unwanted changes in the gathered data. Thus, the GPR performance will be highly influenced by the soil type at which it is sending its electromagnetic waves and receiving the reflected signals. The soil's magnetic, electric and dielectric properties will matter. Four types of soils are shown in Table 1.

Table 1 - Soils Types Composition

	Laterite	Magnetic Sand	Humus A	Humus B
Humus [% of total soil]	0.8	<0.5	2.7	12.4
Clay [%of mineral soil]	31.5	1.3	16.6	17.1
Silt [% of mineral soil]	39.4	7.0	48.4	40.7
Sand [% of mineral soil]	29.1	91.7	35.0	42.2

Figure 1 shows some major types. The most important factors to test in soils are:

- Magnetic susceptibility: soils having very high susceptibility will cause false alarm rates in the metal detectors, because they will change the usual responses of the landmines.
- Electric conductivity: a radar signal cannot propagate to a depth of 20 cm in highly conductive soils, containing salt or clays, because of attenuation.
- Dielectric permittivity: a GPR measures the change in dielectric between soil and buried object. Thus, a change in dielectric permittivity in the soil itself will cause false alarms to occur.
- Soil permeability: determines how well the soil can maintain the moisture and the nutrients, and how much it allows plants to grow in it.

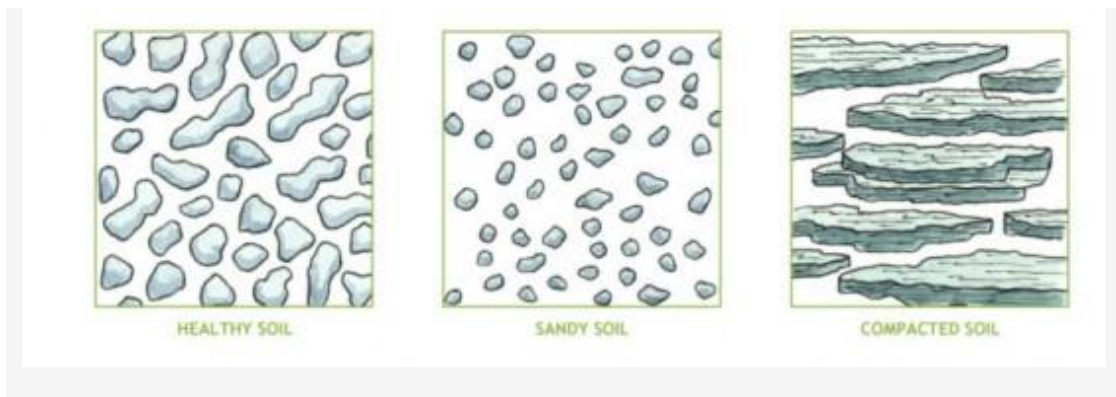


Figure 1 - Major Soil Types

An additional parameter is the soil pH, which is a measure of the acidity or alkalinity of the water held in its pores. The pH scale goes from 0 to 14, with 7 representing neutral. From pH 7 to 0 the soil is increasingly acidic, while from 7 to 14 it is increasingly alkaline.

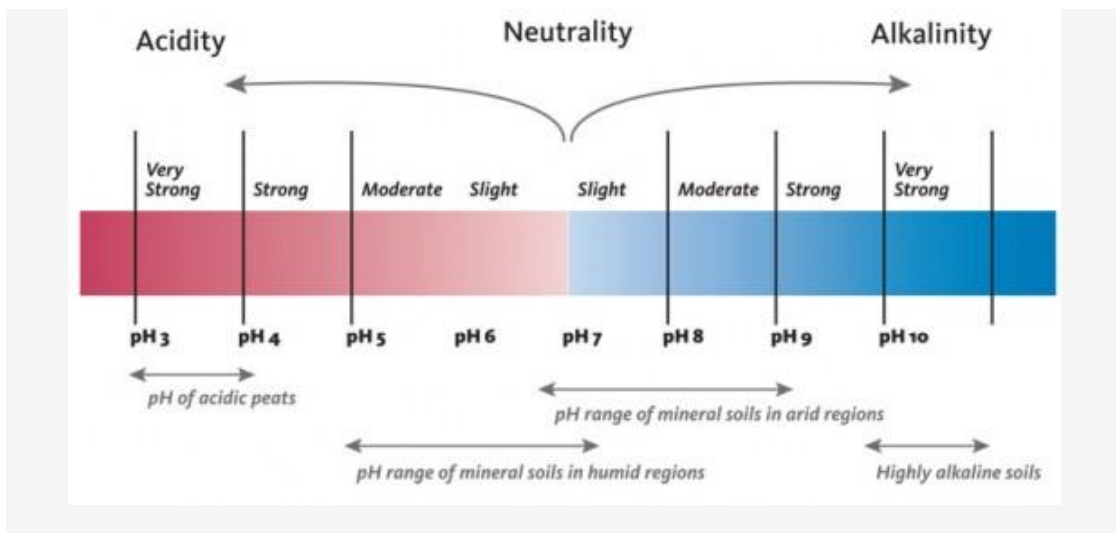


Figure 2 - Soil PH

Soil pH is also a parameter determining whether plants can grow in the soil and benefit from minerals and nutrients. Figure 2 shows the pH distribution for different type of soils with their contents.

The soil structure is a three-phase system which compromises between soil minerals, moisture and air. Moisture being an essential part, determination of the amount of its presence in the soil is a must. Consequently, other properties can vary with the soil moisture, as physical, chemical, mechanical. Hydrological and biological composition of the soil.

The soil moisture itself exists in three forms:

- Gravitational moisture: the moisture that moves in the soil due to gravity. It drains out of the soil three days after the rain fall
- Capillary moisture: the moisture that is held within the soil due to the cohesion and adhesion against the force of gravity.
- Hygroscopic moisture: forms a very thin film around the surface of the soil particles.

Going back to the buried landmines in the soil, in order to determine their presence in a certain area, the type of the soil in which they are buried must be determined. After knowing the soil structure and composition, it will become easier to the researchers to detect landmines with lower false alarm rates.

From this basis, researchers have employed multiple techniques in order to determine the moisture content of the soil. The techniques involve laboratory and in

situ measurements. Some measurement techniques used previously include thermos gravimetric, neutron scattering, soil resistivity and dielectric techniques. Moreover, the amount of moisture held in the soil depends on the particle size distribution, structure of the soil, porosity, specific surface area, depth of the soil, pore fluid characteristics, degree of compaction, organic content, temperature and humidity. Table 2 shows the current developed methods with their specifications and major parameters.

Table 2 - Moisture Determination Methods

Method	Location	Specs	Response time	Measured parameter	Cost \$
Conventional thermo gravimetric technique	In Lab	105°C	24h	Gravimetric soil moisture	400
Neutron moisture meter	In situ	5 MeV energy	2 minutes	Volumetric	10000
TDR	In situ / lab	f=1GHz	28 s	Volumetric	8000
Capacitance technique	In situ / lab	f=10-150MHz	Instant	Volumetric	4000
Resistive sensor	In situ / lab	1-15 atm	3h	Volumetric	30
Thermal dissipation block	In situ / lab	50-200mA	3h	Volumetric	150
Tensiometer	In situ / lab	0-1atm	3h	Suction	75

REFERENCES

- [1] Alzate, L. F.; Ramos, C. M.; Hernández, N. M.; Hernández, S. P.; Mina, N. The vibrational spectroscopic signature of TNT in clay minerals. *Vibrational Spectroscopy* **2006**, 42, 357-368.
- [2] Berhe, A.A. The Contribution of Landmines to Land Degradation. *Land Degradation and Development* **2007**, 18:1-15.
- [3] Beadle, N. C. W. Soil Temperatures During Forest Fires and Their Effect on the Survival of Vegetation. *J. Appl. Ecol.* **1940**, 28, pp. 180-192.
- [4] Solutions for Measuring Permittivity and Permeability with LCR Meters and Impedance Analyzers, Application Note, literature number 5980-2862EN
- [5] Basics of Measuring the Dielectric Properties of Materials, Keysight Technologies, pp.15-31.
- [6] Understanding the Fundamental Principles of Vector Network Analysis, Application Note, literature number 5965-7707E
- [7] John B. Schneider, Understanding the Finite-Difference Time-Domain Method, Chapter 3 pp.33-65, May 25, 2013.
- [8] E.M. Nassar, R. Lee, J.D. Young, A probe antenna for in situ measurements of complex dielectric constant of materials, *IEEE Trans. on Antennas and Propagation*, Vol.47, No:6, pp.1085-1093, 1999.
- [9] E. Yaldiz, M. Baryak, A different method determining dielectric constant of soil and its FDTD simulation, *Mathematical & Computational Applications*, Vol. 8, No:3, pp.303-310, 2003
- [10] W. Skierucha, A. Wilczek, A FDR sensor for measuring complex soil dielectric permittivity in the 10-500 MHz frequency range, *Sensors* 2010, 10, 3314-3329, doi:10.3390/s100403314
- [11] R. Mohan, B. Paul, S. Mridula, P Mohanan, Measurement of soil moisture content at microwave frequencies, *International Conference on Information and Communication Technologies (ICICT 2014)*
- [12] Samir Trabelsi, Andrzej W. Kraszewski, and Stuart O. Nelson, Phase-Shift Ambiguity in Microwave Dielectric Properties Measurements, *IEEE Transactions on Instrumentation and Measurement*. vol. 49. no. I. February 2000
- [13] Suh, Seong-Youp, Warren L. Stutzman, and William Davis, "Multi-broadband

monopole disc antennas,” *2003 IEEE Antennas and Propagation Society International Symposium*, Columbus, OH, June 22–27, 2003, Vol. 3, pp. 616–619.

[14] Agrawall, N. P., et al., “Wide-band planar monopole antennas,” *IEEE Transactions on Antennas and Propagation*, Vol. 46, No. 2, February 1998, pp. 294–295.

[15] Kane Yee (1966). "Numerical solution of initial boundary value problems involving Maxwell's equations in isotropic media". *IEEE Transactions on Antennas and Propagation*. 14 (3): 302–307

[16] J. P. Berenger, “A perfectly matched layer for the absorption of electromagnetic waves,” *J. Comp. Phys.*, vol. 114, no. 2, pp. 185–200, Oct. 1994.

[17] <https://www.remcom.com/>

[18] Hans Gregory Schantz, “Bottom fed planar elliptical UWB antennas”, *Next-RF, Inc. 4811 Cove Creek Drive, Brownsboro, AL35741, IEEE 2003.*

[19] Daniels DJ (ed.) (2004). *Ground Penetrating Radar* (2nd ed.). Knoval (Institution of Engineering and Technology). pp. 1–4. ISBN 978-0-86341-360-5.

[20] M. Chen and C. C. Chen, "UWB in-situ soil permittivity probe with a novel iterative permittivity calibration method," 2012 14th International Conference on Ground Penetrating Radar (GPR), Shanghai, 2012, pp.98-102.

[21] Narayan Prasad Agrawall, Girish Kumar, and K. P. Ray, “Wide-Band Planar Monopole Antennas,” *IEEE Transactions on antennas and propagation*, vol. 46, no. 2, February 1998

[22] Honda, S., M. Ito, H. Seki, and Y. Jinbo, “A disk monopole antenna with 1:8 impedance Bandwidth and omnidirectional radiation pattern,” *Proc. ISAP’92*, Sapporo, Japan, 1992, pp.1145–1148.

[23] Yang, Ning, Zhi Ning Chen, and Xuan Hui Wu, “Study of circular planar monopole for radiosystems,” *Asia-Pacific Microwave Conference*, Vol. 3, November 2003, pp. 1628–1631.

[24] Abul Salam, Mehmet C. Vuran, Xin Dong, Christos Argyropoulos and Suat Irmak, “A Theoretical Model of Underground Dipole Antennas for Communications in Internet of Underground Things’ February 17, 2019